DEPARTMENT OF PHYSICS
UNIVERSITY OF JYVÄSKYLÄ
RESEARCH REPORT No. 5/2010

MICROSCOPIC CALCULATIONS FOR RARE BETA DECAYS

BY
MIKA MUSTONEN

Academic Dissertation
for the Degree of
Doctor of Philosophy

To be presented, by permission of the
Faculty of Mathematics and Natural Sciences
of the University of Jyväskylä,
for public examination in Auditorium FYS1 of the
University of Jyväskylä on May 28, 2010
at 12 o'clock noon

Jyväskylä, Finland
May 2010

Preface

The work presented in this thesis was carried out at the Department of Physics of the University of Jyväskylä (JYFL) during the years 2006–2010. I thank Prof. Jouni Suhonen for introducing me to the fascinating field of theoretical nuclear physics and his patient guidance throughout this project. I also wish to express my gratitude to the examiners of this thesis, Dr. Vadim Rodin and Dr. Vladimir I. Tretyak, who found several misprints that have been corrected in the final version of the manuscript.

There are many people that have greatly influenced me during these years in JYFL. There have been several exceptionally inspiring lecturers, such as (but not limited to) Prof. Kari J. Eskola, Dr. Kimmo Kainulainen, Dr. Sami Räsänen, and Prof. Jacek Dobaczewski. There have been countless fellow students who have shared the passion for trying to understand the nature of Nature sparking eye-opening discussions, and balanced the life with their wonderful sense of humor on a daily basis. All these people have my gratitude.

I gratefully acknowledge the financial support by the University of Jyväskylä, the national Graduate School for Particle and Nuclear Physics (GRASPANP), the Ellen and Artturi Nyyssönen Foundation and the Finnish Cultural Foundation. Their funding has not only paid the roof above my head and the food on my plate, but allowed me to participate in and contribute to conferences both in Finland and abroad.

Finally, I wish to thank my mother and my brother and all my friends for their continuing support and encouragement. My late father repeatedly advised me to educate myself as far as I could. Although I think he meant studying medicine or law, I doubt he would be disappointed his son pursued a PhD in nuclear physics.

Jyväskylä, April 2010

Mika Mustonen

Abstract

In this thesis consisting of six publications and an overview part, three cases of rare beta decays are studied using microscopic nuclear models.

Firstly, the half-lives and electron spectra of ^{113}Cd and ^{115}In fourth-forbidden non-unique ground-state-to-ground-state beta decays are studied using two closely related nuclear models: The microscopic quasiparticle-phonon model (MQPM) and the proton-neutron MQPM (pnMQPM), which has been developed as a part of this thesis work. Our results for these rare decays are compared to the available experimental data and are found to agree reasonably well.

As the second application, the partial half-lives of the yet unobserved single-beta decay channels competing with the double beta decay of ^{96}Zr are computed to estimate the possible contamination from these channels to the geochemical double-beta-decay experiments. According to our results obtained by applying the proton-neutron quasiparticle random-phase approximation (pnQRPA), the error stemming from them is still within the experimental uncertainties of the geochemical experiments.

Finally, the recently discovered tiny ultra-low-Q-value decay branch of ^{115}In has been investigated in collaboration with the JYFLTRAP group in Jyväskylä and the HADES underground laboratory in Belgium. Our pnMQPM prediction for the half-life is found to differ from the experimentally obtained result by more than an order of magnitude. The various atomic contributions possibly responsible for this discrepancy are discussed.

Author's address Mika Mustonen
Department of Physics
University of Jyväskylä
Finland

Supervisor Professor Jouni Suhonen
Department of Physics
University of Jyväskylä
Finland

Reviewers Doctor Vadim Rodin
Institut für Theoretische Physik
University of Tübingen
Germany

Doctor Vladimir I. Tretyak
Institute for Nuclear Research
National Academy of Sciences of Ukraine
Ukraine

Opponent Professor Osvaldo Civitarese
Department of Physics
University of La Plata
Argentina

List of Publications

I M. T. Mustonen, M. Aunola and J. Suhonen, *Theoretical description of the fourth-forbidden non-unique β decays of ^{113}Cd and ^{115}In* Phys. Rev. C **73**, 054301 (2006); erratum Phys. Rev. C **76**, 019901(E) (2007).

II H. Heiskanen, M. T. Mustonen and J. Suhonen, *Theoretical half-life for beta decay of ^{96}Zr* J. Phys. G: Nucl. Part. Phys. **34**, 837-843 (2007)

III M. T. Mustonen and J. Suhonen, *Microscopic quasiparticle-phonon description of beta decays of ^{113}Cd and ^{115}In using proton-neutron phonons* Phys. Lett. B **657**, 38-42 (2007)

IV J. S. E. Wieslander, J. Suhonen, T. Eronen, M. Hult, V.-V. Elomaa, A. Jokinen, G. Marissens, M. Misiaszek, M. T. Mustonen, S. Rahaman, C. Weber, and J. Äystö, *The smallest known Q value of any nuclear decay: the rare β^- decay of ^{115}In $(9/2^+) \rightarrow {}^{115}Sn$ $(3/2^+)$* Phys. Rev. Lett. **103**, 122501 (2009)

V M. T. Mustonen and J. Suhonen, *Forbidden beta decays of ^{96}Zr and ^{115}In: Implications for neutrino physics* AIP Conf. Proc. **1180**, 76-80 (2009).

VI M. T. Mustonen and J. Suhonen, *Nuclear and atomic contributions to beta decays with ultra-low Q values* J. Phys. G: Nucl. Part. Phys. **37**, 064008 (2010).

The author has derived the formulas for Hamiltonian matrix elements and transition densities in the proton-neutron quasiparticle-phonon model (pnMQPM). The author has written the computer programs for solving the pnMQPM equations, calculating the charge-changing transition densities and evaluating the formulas for highly-forbidden beta decays. The author has carried out the theoretical calculations for publications I, III, IV and VI and written the first draft for publications I, III, V and VI. The author has also contributed to several conference proceedings not included in this thesis.

Contents

1 Introduction

Nuclear physics, born a century ago in the famous Rutherford experiment revealing the unexpected existence of the atomic nucleus, still holds many mysteries. The nuclear beta decay is often considered a well-understood part of the nuclear theory. This thesis work concentrates on a few extreme cases of rare beta decays which had not been studied theoretically before.

The single-beta-decay studies are currently not very fashionable, the spotlight shining on the double-beta-decay experiments promising to uncover the true nature of the neutrino – whether it is its own antiparticle or not – as well as its mass. The nuclides studied in the present work are of interest to the experimentalists because of their possible applications in neutrino physics and double-beta-decay studies. ^{115}In has been envisioned as a real-time detector material for the LENS experiment [1] aiming to measure the Sun's neutrino luminosity to high precision and hence push forward to expand our knowledge of both our own star and the physics of neutrinos. The COBRA[1] double-beta-decay experiment [2] has used ^{113}Cd beta decay as one of the test experiments for their room-temperature CdZnTe semiconductor detectors [3]. In ^{96}Zr, the single beta decay competes with the double beta decay, and is a possible error source for the geochemical measurement of the double-beta-decay half-life.

There exists no practicable nuclear model capable of predicting every observable of every one of the thousands of known nuclides[2]. To be able to compute quantities which could be compared to experimental results, a nuclear theorist needs to simplify the nuclear many-body problem by introducing one approximation after another while preserving the essential features of the nucleus. This leads to a myriad of nuclear models, each with distinct capabilities and limitations arising from the chosen approximations.

There are many microscopic models based on different ways of coupling BCS quasiparticles and phonons to form the configuration basis and deriving the Hamiltonian, such as the quasiparticle-phonon nuclear model (QPNM) [5], the microscopic anharmonic vibrator approach (MAVA) [6], its proton-neutron variant (pnMAVA) [7] and the microscopic quasiparticle-phonon model (MQPM) [8]. As a part of this thesis project, the proton-neutron quasiparticle-phonon model (pnMQPM) was developed

[1] "Cadmium-zinc-telluride 0-neutrino double-Beta Reseach Apparatus".

[2] In February 3rd 2010, the total number of nuclides in the NuDat 2 database [4] of Brookhaven National Laboratory was 3175.

as yet another tool to complement this arsenal. Its aim is to better describe the weak-interaction processes such as beta decay and neutrino scattering in odd-mass medium-heavy to heavy spherical (or nearly spherical) nuclei.

2 Describing the nuclear structure

Many difficulties in solving the nuclear many-body problem arise from the inconvenient number of particles. Except for the very lightest nuclei, there are too many particles involved for the problem to be solved by exact methods. Yet there are too few particles in a nucleus for a good statistical description. The interaction between the nucleons is strong and still only approximately known, making the problem even more challenging. The mean-field approximation has been found to be a successful starting point for tackling the nuclear many-body problem.

2.1 Nuclear mean field

In the mean-field approximation nucleons are considered as independent particles moving in the nuclear mean field created by the other nucleons in the nucleus. More formally, to solve the many-body Hamiltonian $H = T + V$, where T stands for the kinetic energy and V for the potential energy terms, a mean-field potential $V_{\text{m.f.}}$ is chosen so that both the Hamiltonian $H_{\text{m.f.}} = T + V_{\text{m.f.}}$ is solvable and the residual interaction $V_{\text{res}} = V - V_{\text{m.f.}}$ is sufficiently small that one can apply the pertubation theory. Essentially this approach converts the problem of strongly interacting particles to the easier problem of weakly interacting mean-field *quasiparticles*.

The mean field potential can be generated e.g. by the iterative Hartree-Fock procedure. Alternatively, an effective potential can be taken as the mean field: for example the harmonic oscillator potential or, as in this work, the more realistic phenomenological Woods-Saxon potential (Figure 2.1)

$$v_{\text{WS}}(r) = -\frac{V_0}{1 + e^{(r-R)/a}}, \tag{2.1}$$

where we have adopted the parametrization of Ref. [9]: $R = 1.27 \text{ fm} \times A^{1/3}$ for the nuclear radius, $a = 0.67$ fm for the surface diffuseness and

$$V_0 = \left(51 \pm 33\frac{N-Z}{A}\right) \text{ MeV}, \tag{2.2}$$

where the plus sign is selected for protons and the minus sign for neutrons, for the depth of the potential. The Woods-Saxon potential is known to successfully reproduce

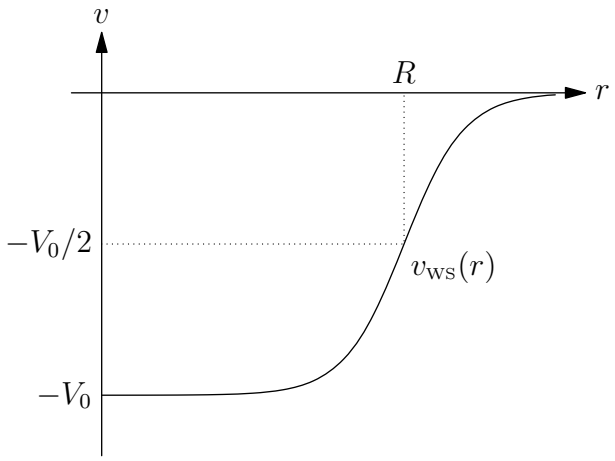

Figure 2.1: Schematic picture of the Woods-Saxon potential $v_{\mathrm{WS}}(r)$. The parameter V_0 is the depth of the potential, R the nuclear radius and a controls the surface diffuseness.

the observed shell structure in the nuclei, when the spin-orbit interaction is taken into account. For protons the Coulomb interaction must also be included, but it does not modify the shell structure as dramatically.

In the calculations of this work, some energies of the mean-field states near the Fermi surface have been adjusted by hand so that the BCS quasiparticle spectrum better agrees with the experimental energy level data. This is justified since the Woods-Saxon potential is a global parametrization for the mean-field. Special care has been taken so that no unphysical adjustments, such as changing the order of spin-orbit partners[1], are made.

The problem is further simplified by including only a limited set of single-particle states in the valence space. In this work, the valence space is selected so that it contains two to three major shells (see Chapter 4) around the Fermi levels for protons and neutrons. The fully occupied states below the valence space in energy are approximated as an inert *core* that does not directly interact with the valence space particles.

[1]Spin-orbit partners differ in total angular momentum by one unit but share the same principal quantum number n and the same orbital angular momentum quantum number l, for example $1\mathrm{d}_{3/2}$ and $1\mathrm{d}_{5/2}$.

2.2 Bardeen-Cooper-Schrieffer theory for nuclei

There is plenty of experimental evidence of the pairing phenomenon in nuclei, i.e. the tendency of the nuclear Hamiltonian to favour pairs of nucleons coupled to zero total angular momentum. Perhaps the most striking example of such evidence is the fact that the ground-state of every known even-even nucleus has the angular momentum and parity 0^+. Other evidence include e.g. the energy gap between the ground state and the lowest excitations present only in the even-even nuclei and the odd-even effect. The analogy to the Cooper pairs in the Bardeen-Cooper-Schrieffer (BCS) theory for superconducting metals [10] was quickly recognized in the late 1950's by Bohr, Mottelson and Pines [11], and the BCS approach adapted to nuclei soon became one of the standard tools of microscopic nuclear theory.

The BCS quasiparticle creation and annihilation operators are formed as linear combinations of the mean-field quasiparticle creation and annihilation operators[2]

$$\begin{cases} a_\beta^\dagger = u_b c_\beta^\dagger + v_b \tilde{c}_\beta \\ \tilde{a}_\beta = u_b \tilde{c}_\beta - v_b c_\beta^\dagger \end{cases} . \tag{2.3}$$

This is known as the Bogolyubov-Valatin transformation after the two physicists who first introduced it in [12, 13]. Here the notation of Baranger [14] is adopted: A Roman index stands for the set of the principal quantum number n, the orbital angular momentum l and the total angular momentum j, e.g. $b = \{n_b, l_b, j_b\}$. The corresponding Greek index also includes the projection quantum number m, so that e.g. $\beta = \{n_b, l_b, j_b, m_\beta\}$. The operator $c_\beta^\dagger$ is the particle creation operator and $\tilde{c}_\beta = (-1)^{j_b + m_\beta} c_{-\beta}$, where $-\beta = \{n_b, l_b, j_b, -m_\beta\}$, is the corresponding time-reversed annihilation operator. The occupation amplitude v_b and the unoccupation amplitude u_b are to be solved via a variational procedure where the ground-state energy is minimized (See e.g. [15] for details).

The BCS ground state, formally written as the ansatz

$$|\mathrm{BCS}\rangle = \prod_{\alpha>0} (u_a - v_a c_\alpha^\dagger \tilde{c}_\alpha^\dagger) \, |\mathrm{CORE}\rangle \, , \tag{2.4}$$

acts as the vacuum for the quasiparticles. The index α runs over all the like-nucleon states having a positive projection quantum number m_α. The $|\mathrm{CORE}\rangle$ represents the inert nuclear core, i.e. the filled single-particle states energetically below the selected model space. The particle number is not a good quantum number for the BCS ground state. The condition that the *average* particle number equals to the number of valence

[2] From this point on in this thesis the BCS quasiparticles are referred to as *quasiparticles* and the mean-field quasiparticles simply as *particles*.

nucleons in the reference nucleus, ground state of which the BCS vacuum is aimed to describe, is used as a constraint in the variational procedure.

The nuclear Hamiltonian with a two-particle interaction is

$$H = \sum_{\alpha} \varepsilon_{\alpha} c_{\alpha}^{\dagger} c_{\alpha} + \frac{1}{4} \sum_{\alpha\beta\gamma\delta} \bar{v}_{\alpha\beta\gamma\delta} c_{\alpha}^{\dagger} c_{\beta}^{\dagger} c_{\delta} c_{\gamma}, \tag{2.5}$$

where the antisymmetrized two-body matrix elements $\bar{v}_{\alpha\beta\gamma\delta}$ are obtained in this work from the Bonn one-boson-exchange potential using the G-matrix technique [16]. When the Hamiltonian is transformed to the quasiparticle picture using the Bogolyubov-Valatin transformation, it takes the form

$$H = H_{11} + H_{20} + H_{02} + H_{22} + H_{40} + H_{04} + H_{31} + H_{13}, \tag{2.6}$$

where each term H_{mn} is proportional to a normal-ordered product of m quasiparticle creation and n quasiparticle annihilation operators. The ground-state energy term has been omitted since only the relative energies of the states are of interest in this work. The minimization of the ground-state energy in the BCS procedure causes the terms H_{20} and H_{02} to vanish. Physically this means that there are no quasiparticle pair excitations across the Fermi surface. This indicates that the transformation absorbs a large part of the residual interaction V_{res} into the very structure of the quasiparticles.

In the BCS calculations of this work the interaction matrix elements were scaled by a constant g_{pair} for protons and neutrons separately so that the lowest quasiparticle energy matched the experimental pairing gap, which was calculated from the experimental separation energies of [17, 18, 19, 20, 21] using the linear approximation formulas of [22]. These adjustments were small in all our applications, i.e. the scaling constants g_{pair} were close to unity.

2.3 Proton-neutron quasiparticle random-phase approximation

The proton-neutron quasiparticle random-phase approximation (pnQRPA) [23] describes the states of the adjacent isobars of the BCS reference nucleus as proton-neutron-quasiparticle-pair excitations. These excitations, called pnQRPA phonons, are created by the operator

$$Q_{\omega}^{\dagger} = \sum_{pn} \left(X_{pn}^{\omega} \left[a_p^{\dagger} a_n^{\dagger} \right]_{J_\omega M_\omega} + Y_{pn}^{\omega} \left[\tilde{a}_p \tilde{a}_n \right]_{J_\omega M_\omega} \right), \tag{2.7}$$

where the index ω contains the angular momentum J_ω, the projection quantum number M_ω and the parity π_ω of the phonon, and the additional index k_ω enumerating

the different states with the same J_ω, M_ω and π_ω. The forward-going amplitude X^ω_{pn} and the backward-going amplitude Y^ω_{pn} are to be determined by diagonalizing the pnQRPA Hamiltonian. In the quasi-boson approximation the pnQRPA phonon creation and annihilation operators satisfy the commutation relations

$$\left[Q_\omega, Q^\dagger_{\omega'}\right] \cong \delta_{\omega\omega'} \text{ and } \left[Q_\omega, Q_{\omega'}\right] = 0 = \left[Q^\dagger_\omega, Q^\dagger_{\omega'}\right] \tag{2.8}$$

and act therefore to a good approximation as bosons.

The pnQRPA ground state is defined as the vacuum for the pnQRPA phonons, i.e.

$$Q_\omega \left|\text{pnQRPA}\right\rangle = 0. \tag{2.9}$$

The pnQRPA ground state is approximately equal to the BCS ground state as long as the backward-going amplitudes remain significantly smaller than the forward-going ones. If the requirement $|Y^\omega_{pn}| \ll |X^\omega_{pn}|$ is not met, the RPA description breaks down.

The pnQRPA equations can be derived using the equations-of-motion method [24], and they can be written in a convenient matrix form

$$\begin{pmatrix} A & B \\ -B^* & -A^* \end{pmatrix} \begin{pmatrix} X^\omega \\ Y^\omega \end{pmatrix} = E_\omega \begin{pmatrix} X^\omega \\ Y^\omega \end{pmatrix}. \tag{2.10}$$

A useful procedure for solving eigenvalue problems of this type, developed by Ullah and Rowe [25], is applied in our computational codes.

In our applications to ^{113}Cd and ^{115}In, the pnQRPA spectra were fine-tuned to better correspond to the experimentally observed energy spectra by scaling the interaction matrix elements by the constants g_{pp} (particle-particle matrix elements) and g_{ph} (particle-hole matrix elements). However, the final results of the beta decay calculations were not sensitive to these adjustments in any of our applications. The corresponding procedure was used for scaling the QRPA matrix elements in the MQPM calculation [8].

The pnQRPA is known to satisfy the Ikeda sum rule [26]. This fact motivated us to develop a variation of the MQPM using the pnQRPA phonons instead of the QRPA phonons hoping that it might improve the description of the weak-interaction transitions, such as beta decays and neutrino-nucleus scattering reactions.

2.4 Proton-neutron microscopic quasiparticle-phonon model

In the microscopic quasiparticle-phonon model (MQPM), first presented in [27] and further refined in [8], the basis of the states of a fixed total angular momentum and

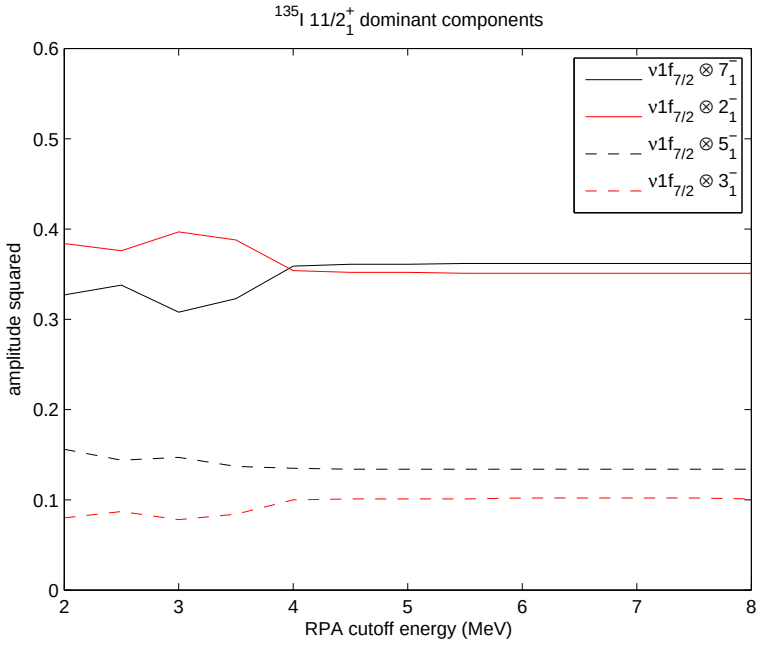

Figure 2.2: Squared amplitudes of the four largest components of the ^{135}I lowest $11/2^+$ state pnMQPM wave function as functions of the cut-off energy for the pnQRPA phonons. The convergence at 4 MeV corresponds to 51 pnQRPA phonons.

parity j^π consists of the one-quasiparticle states and three-quasiparticle states constructed by coupling one-quasiparticle states and QRPA phonons to j^π. The proton-neutron variant of the MQPM (pnMQPM) takes the same approach but using the pnQRPA phonons. The pnMQPM excitation operator reads

$$\Gamma_i(jm) = \sum_p C_p^i a_{p,m}^\dagger + \sum_{n\omega} D_{n\omega}^i \left[a_n^\dagger Q_\omega^\dagger\right]_{jm} \tag{2.11}$$

or

$$\Gamma_i(jm) = \sum_n C_n^i a_{n,m}^\dagger + \sum_{p\omega} D_{p\omega}^i \left[a_p^\dagger Q_\omega^\dagger\right]_{jm} \tag{2.12}$$

in the case of the proton-odd or the neutron-odd nucleus, respectively. Naturally, the first summation runs over only those quasiparticle states that have the angular momentum and parity j^π, and the second one over the combinations of quasiparticles and phonons that can be coupled to j^π. The amplitudes C_a^i and $D_{a\omega}^i$ are to be determined by diagonalizing the Hamiltonian.

In practice, the basis is truncated by taking into account only the lowest-energy phonons. This is physically justified, since the high-energy states are expected to interfere very little with the low-lying states. A suitable cut-off value for the phonon energy was found by observing the convergence of the amplitudes of the dominant

configurations in the wave functions of the states of interest. This is illustrated by the example in Figure 2.2. The example also demonstrates the typical situation that the pnMQPM wave functions for three-quasiparticle states tend to consist of two to four major components, whereas the corresponding MQPM wave functions usually have a clear dominant component. In this sense the MQPM description is more natural, as the MQPM basis states are closer to the energy eigenstates than the pnMQPM ones.

The one-quasiparticle states are orthogonal to each other and to the three-quasiparticle states. However, the three-quasiparticle states are not orthogonal to each other and form an overcomplete set. The overlap between two three-quasiparticle states is

$$\left\langle \left| \left[a^\dagger_{n'} Q^\dagger_{\omega'}\right]^\dagger_{jm} \left[a^\dagger_n Q^\dagger_\omega\right]_{jm} \right| \right\rangle = \delta_{nn'}\delta_{\omega\omega'} + K^{(p)}(n\omega n'\omega'; j) \tag{2.13}$$

in the case of the neutron-odd nucleus or

$$\left\langle \left| \left[a^\dagger_{p'} Q^\dagger_{\omega'}\right]^\dagger_{jm} \left[a^\dagger_p Q^\dagger_\omega\right]_{jm} \right| \right\rangle = \delta_{pp'}\delta_{\omega\omega'} + (-1)^{j_p+j_{p'}+J_\omega+J_{\omega'}+1} K^{(n)}(p\omega p'\omega'; j) \tag{2.14}$$

in that of the proton-odd nucleus. The auxiliary expressions $K^{(p)}(n_1\omega_1 n_2\omega_2; j)$ and $K^{(n)}(p_1\omega_1 p_2\omega_2; j)$ are defined as

$$K^{(p)}(n_1\omega_1 n_2\omega_2; j) = \widehat{J_{\omega_1}}\widehat{J_{\omega_2}} \sum_p \left(\begin{Bmatrix} j & j_{n_1} & J_{\omega_1} \\ j_p & j_{n_2} & J_{\omega_2} \end{Bmatrix} X^{\omega_2}_{pn_1} X^{\omega_1}_{pn_2} - \frac{\delta_{jj_p}}{\widehat{j^2}} Y^{\omega_2}_{pn_2} Y^{\omega_1}_{pn_1} \right) \tag{2.15}$$

and

$$K^{(n)}(p_1\omega_1 p_2\omega_2; j) = \widehat{J_{\omega_1}}\widehat{J_{\omega_2}} \sum_n \left(\begin{Bmatrix} j & j_{p_1} & J_{\omega_1} \\ j_n & j_{p_2} & J_{\omega_2} \end{Bmatrix} X^{\omega_2}_{p_1 n} X^{\omega_1}_{p_2 n} - \frac{\delta_{jj_n}}{\widehat{j^2}} Y^{\omega_2}_{p_2 n} Y^{\omega_1}_{p_1 n} \right). \tag{2.16}$$

The equations-of-motion method [24] leads to the generalized eigenvalue equation

$$H\psi_k = E_k N \psi_k, \tag{2.17}$$

where the matrix N is the overlap matrix, H is the Hamiltonian matrix and ψ_k is the eigenvector corresponding to the energy eigenvalue E_k. The components of ψ_k are the coefficients C^k_p and $D^k_{n\omega}$ (or C^k_n and $D^k_{p\omega}$) of Eqs. (2.11) and (2.12).

The Hamiltonian matrix elements in the pnMQPM basis are listed in Appendix A. The MQPM and the pnMQPM share the important feature that they both start from the Hamiltonian of Eq. (2.6) with simple interpretation of its terms: Interaction between two phonons (H_{22}), between one-quasiparticle and three-quasiparticle configurations (H_{31}+H_{13}) etc. All these terms are treated on equal footing, differentiating the MQPM and the pnMQPM from many other quasiparticle-phonon approaches.

The differences between the MQPM and pnMQPM arise from two factors: Firstly, the three-quasiparticle part of the configuration space is different between these two

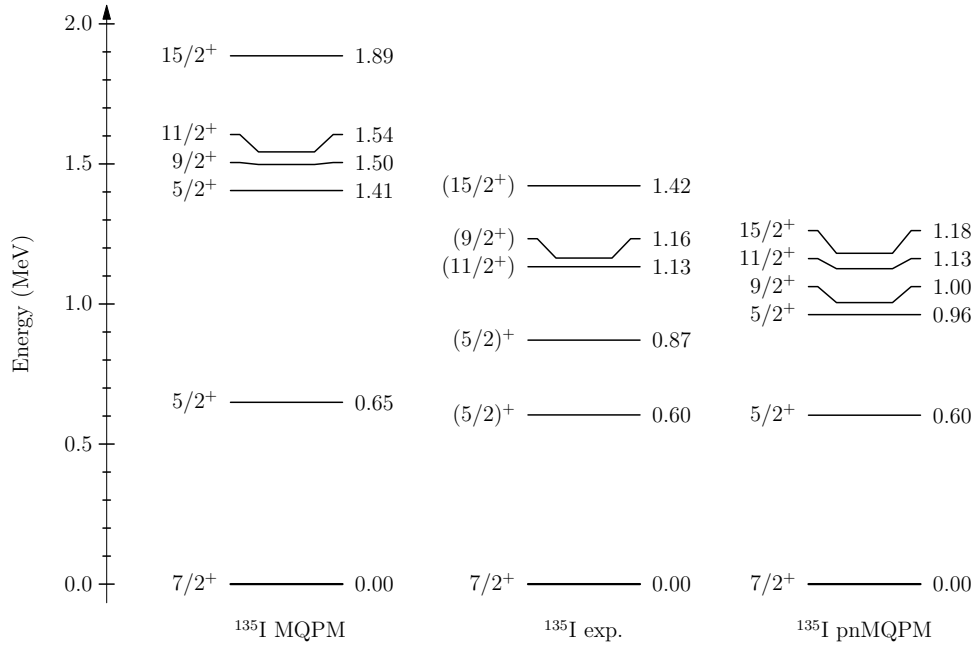

Figure 2.3: The MQPM description of ^{135}I suffers from the problematic 2_1^+ QRPA state of ^{134}Te, but the pnMQPM circumvents this problem by using the pnQRPA excitations instead. Only the states with known or tentative spin-parity assignment up to 1.5 MeV are included in the experimental spectrum, and only the corresponding theoretical states are included for the MQPM and the pnMQPM. The MQPM results are from [28] and the experimental spectrum from [29].

models. For a proton-odd nucleus, the MQPM three-quasiparticle configuration space contains the three-proton configurations and one-proton-two-neutron configurations. In the pnMQPM only one-proton-two-neutron configurations are included due to the proton-neutron structure of the pnQRPA excitation. This is the primary weakness of the pnMQPM model, and for the states where three-proton contributions are important, the pnMQPM description is inevitably inaccurate.

The second difference is that in the RPA step the adjustments are made to a different set of experimental data. This can be an advantage to the pnMQPM, when there are problems describing the reference nucleus spectrum using the QRPA. One example of such a case is ^{135}I, where the MQPM fails to produce the correct energy spectrum due to the too high QRPA energy of ^{134}Te 2_1^+ state [28]. This nucleus was used as one of our early test cases for the pnMQPM; the results for the lowest states are presented in Figure 2.3.

Our adopted method [30] for dealing with the overcompleteness of the pnMQPM basis is the same as the one used with the MQPM. First the overlap matrix N is diagonalized to find a new, orthogonal basis:

$$Nu^{(k)} = n_k u^{(k)}, \tag{2.18}$$

where the index k enumerates the different eigenstates. Ideally, the states to be discarded as spurious would have a zero eigenvalue. However, due to the fact that not all the pnQRPA phonons are used in building the basis, and also (less importantly) to the fact that there is likely to be some numerical inaccuracy, these states often have a small non-zero eigenvalue. In practice, one needs to set a suitable upper limit for the eigenvalues which are to be discarded. The physical validity of the choice for this cut-off value was monitored in our application by substitution of the computed wave functions back in the original generalized eigenvalue equation.

The new complete set of orthonormal basis states are

$$|\tilde{k}\rangle = \frac{1}{\sqrt{n_k}} \sum_i u_i^{(k)} |i\rangle \,, \tag{2.19}$$

where the tilde emphasizes that the vector belongs to the set of new basis vectors, and the index i runs over the basis states of the overcomplete basis. In the new basis the original generalized eigenvalue equation transforms into an ordinary eigenproblem

$$\tilde{H} g^{(v)} = \lambda_v g^{(v)}, \tag{2.20}$$

where the Hamiltonian matrix elements in the new basis are

$$\tilde{H}_{ab} = \frac{1}{\sqrt{n_a n_b}} \sum_{ij} (u_i^{(a)})^* u_j^{(b)} \langle i| H |j\rangle \,. \tag{2.21}$$

The eigenvalues λ_v are now the energies of the (pn)MQPM states. The (unnormalized) coefficients of the (pn)MQPM wave functions in the original basis can be identified from the equation

$$|v\rangle = \sum_i \underbrace{\sum_a g_a^{(v)} \frac{1}{\sqrt{n_a}} u_i^{(a)}}_{C_i^v \text{ or } D_i^v} |i\rangle \,, \tag{2.22}$$

where again the index i runs over the basis vectors of the overcomplete basis and a runs over the dimension of the restricted complete basis.

3 Nuclear beta decay

The general formalism of the beta-decay theory is developed in detail in the comprehensive treatment by Behrens and Bühring [31]. Less detailed introductions to calculating the allowed and unique forbidden decays can be found in many text books, e.g. in [15]. In this chapter the general beta-decay theory of [31] is superficially introduced and the results of [31] are connected to the nuclear models used in this work.

The famous first theoretical work to quantitatively explain the beta decay was the theory by Fermi [32]. It was inspired by the quantum-mechanical treatment of electromagnetic radiation, and consequently the form of a vector interaction was assumed for the decay mechanism. Pauli's neutrino hypothesis was a key ingredient in the theory, and its success lead to the general acceptance of the elusive particle's existence long before it was experimentally observed. Fermi's theory was soon extended by Gamow and Teller [33] by including the possibility of emitting the electron-neutrino pair in a spin triplet state. After the discovery of the parity violation in the beta-decay experiment by Wu *et al* [34], the phenomenological theory for beta decay reached its final vector-minus-axial-vector ("$V - A$") form.

Unlike the quantum electrodynamics, the $V - A$ theory is not renormalizable. This problem was solved by the gauge theory unifying the weak and electromagnetic interaction introduced by Glashow, Weinberg and Salam (See e.g. [35]). Predictions of this electroweak theory have been verified by countless experiments, and the one experimentally yet unobserved particle predicted by the theory, the famous *Higgs boson*, is expected to reveal itself in the Large Hadron Collider (LHC) experiment at CERN.

3.1 Phenomenological $V - A$ theory

In the standard model of electroweak interactions, the beta decay is a semi-leptonic process mediated by a charged gauge boson W^- or W^+ (See Figure 3.1). Due to the high mass of the gauge bosons (roughly 80 GeV), the weak interaction has an extremely short range: it is point-like even on the nuclear scale. From the nuclear-theory point of view it is a very good approximation to consider it as an effective four-point interaction. This phenomenological vector-minus-axial-vector ("$V - A$") interaction of the hadronic and the leptonic current has proven to be a tractable approach at the low energies of the nuclear beta decay.

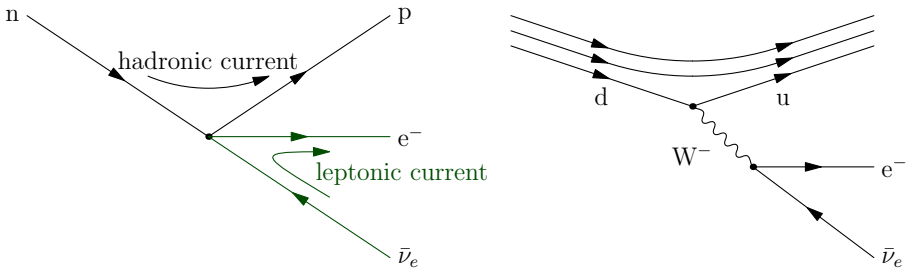

Figure 3.1: Beta minus decay viewed as a current-current interaction in the phenomenological $V-A$ theory (left) and as the standard-model weak interaction mediated by the W^- boson on the quark level (right).

For the leptonic current the vector coupling and the axial vector coupling are of the same strength, but due to the internal structure of the hadrons and the renormalization effects of the strong interaction, the axial-vector coupling is modified in the case of the hadronic current. The renormalization of the hadronic axial-vector current is, however, small in the sense that the value of the axial-vector coupling constant g_{A} is not far from unity. In this work, the value $g_{\mathrm{A}} = 1.25$ is adopted. The fact that the axial current is only slightly renormalized is known in the standard model as the partially conserved axial-vector current (PCAC) hypothesis.

The vector part of the current is nevertheless unmodified by the presence of the strong interaction. It is believed to be "protected" by the electromagnetic interaction [36]. This is known as the conserved vector current (CVC) hypothesis, and it asserts that the value of the vector coupling constant is $g_{\mathrm{V}} = 1$.

More formally, the Hamiltonian density in the $V - A$ theory of beta decay is

$$H_\beta(x) = -\frac{G_{\mathrm{F}}}{\sqrt{2}}\big[\underbrace{\bar{\psi}_p(x)\gamma_\mu(1+\lambda\gamma_5)\psi_n(x)}_{J^\dagger_\mu(x)}\underbrace{\bar{\psi}_e(x)\gamma^\mu(1-\gamma_5)\psi_\nu(x)}_{L^\mu(x)} + \mathrm{H.c.},\big] \tag{3.1}$$

where $J_\mu(x)$ is the hadron current (the nuclear current) and $L_\mu(x)$ is the lepton current operator. The constant G_{F} is the Fermi coupling constant. The constant $\lambda = -g_A/g_V$ in the hadron current operator is the ratio between the axial-vector and vector coupling constants discussed above.

3.2 General formalism for β^- decays

The probability for emitting an electron with the total energy in the interval $[W_e, W_e + dW_e]$ is

$$P(W_e)dW_e = \frac{G_F^2}{(\hbar c)^6}\frac{1}{2\pi^3\hbar}F_0(Z,W_e)C(W_e)\,p_e c\,W_e(W_0 - W_e)^2\,dW_e, \tag{3.2}$$

where Z is the charge of the daughter nucleus, $p_e = \sqrt{W_e^2 - (m_e c^2)^2}$ is the electron momentum and W_0 is the maximum total energy of the electron. The Fermi function $F_0(Z, W_e)$ approximates the effect of the Coulomb interaction between the nucleus and the emitted electron on the beta spectrum. It is defined as the ratio of the absolute squares of the relativistic Coulomb wave function and the free lepton wave function at the nuclear radius [15]. Introducing modifications to the Fermi function is the natural way of taking atomic corrections into account, for example by the Rose prescription [37] where the electron screening is taken into account by replacing the Fermi function with

$$F_0^{\text{screened}}(Z,W_e) \approx \frac{\tilde{p}_e\tilde{W}_e}{p_e W_e}F_0(Z,W_e), \tag{3.3}$$

where $\tilde{W}_e = W_e - V_0$ and $\tilde{p}_e = \sqrt{\tilde{W}_e^2 - (m_e c^2)^2}$. Here V_0 is the difference between the Coulomb potential energy and the exact potential energy of the continuum electron at the nuclear radius, and it has been studied in more detail in [38]. The shape factor $C(W_e)$ contains the details of the nuclear structure. It is a constant for allowed decays, and in the case of forbidden decays it modifies the beta spectrum shape in addition to the total decay probability. The kinematical factor $p_e c\,W_e(W_0 - W_e)^2\,dW_e$ arises from the available final-state-lepton phase space with the approximation of zero neutrino mass.

Integrating the probability density (3.2) over all possible electron energies yields the decay rate, and the half-life is then simply

$$T_{1/2} = \kappa\left((m_e c^2)^{-5}\int_{m_e c^2}^{W_0} F_0(Z,W_e)C(W_e)\,p_e c\,W_e(W_0 - W_e)^2\,dW_e\right)^{-1}. \tag{3.4}$$

Formally the constant κ is

$$\kappa = \frac{2\pi^3\hbar\ln 2}{(m_e c^2)^5 G_{\mathrm{F}}^2/(\hbar c)^6}, \tag{3.5}$$

but in practice it is slightly renormalized by the so-called inner radiative corrections. Therefore it is more accurate to use the value $\kappa = 6147$ s obtained from an extensive survey of superallowed β decays [39].

To evaluate the shape factor, the first step in the treatment of [31] is to make a multipole expansion of the nuclear current

$$(-i)\langle f|V_\mu(0)+A_\mu(0)|i\rangle\gamma_0\gamma^\mu = \sum_{KLMS}(-1)^{J_f-M_f+M}(-i)^L\sqrt{4\pi}\widehat{J}_i \times \begin{pmatrix} J_f & K & J_i \\ -M_f & M & M_i \end{pmatrix} T^{-M}_{KLS}(\hat{q})\frac{(qR/\hbar)^L}{(2L+1)!!}F_{KLS}(q^2), \quad (3.6)$$

where q is the momentum transfer, R is the nuclear radius, $T^{-M}_{KLS}(\hat{q})$ is an operator acting on the lepton spinors and $F_{KLS}(q^2)$ are the nuclear *form factors* containing all the details of the nuclear structure. The form factors are then expanded as a power series

$$F_{KLS}(q^2) = \sum_n \frac{(-1)^n(2L+1)!!}{(2n)!!(2L+2n+1)!!}\left(\frac{qR}{\hbar}\right)^{2n}F^{(n)}_{KLS}. \quad (3.7)$$

Due to the huge mass of the nucleus compared to the electron, the momentum transfer q is so small that a form factor can be approximated with its leading term[1] $F^{(0)}_{KLS} = F_{KLS}(q=0)$. Taking the non-zero nuclear charge into account also introduces additional form factors $F^{(0)}_{KLS}(k_e,1,1,1)$, which are sensitive to the electron relativistic quantum number k_e and the nuclear charge distribution. In this work, a uniform spherical charge distribution is assumed for the nucleus.

The form factors enter the formulas for observables only as certain highly complicated linear combinations $M_K(k_e,k_\nu)$ and $m_K(k_e,k_\nu)$. The beta-decay shape factor has the form

$$C(W_e) = \sum_{k_e k_\nu K}\frac{F_{k_e-1}(Z,W_e)}{F_0(Z,W_e)}\left[M^2_K(k_e,k_\nu)+m^2_K(k_e,k_\nu) - \frac{2\mu_{k_e}\gamma_{k_e}}{k_eW_e/(m_ec^2)}M_K(k_e,k_\nu)m_K(k_e,k_\nu)\right], \quad (3.8)$$

where K is the transfered angular momentum and k_e and k_ν are the absolute values of the relativistic electron and neutrino quantum numbers κ_e and κ_ν. The Coulomb function μ_{k_e} can be approximated as unity in the case of the nuclear beta decay and $\gamma_{k_e} = \sqrt{k_e^2-(\alpha Z)^2}$, where α is the fine-structure constant. $F_{k_e-1}(Z,W_e)$ is the generalized Fermi function, for which we use the definition

$$F_{k-1}(Z,W_e) = 4^{k-1}(2k)(k+\gamma_k)[(2k-1)!!]^2e^{\pi y}\left(\frac{2p_eR}{\hbar}\right)^{2(\gamma_k-k)}\left(\frac{|\Gamma(\gamma_k+iy)|}{\Gamma(1+2\gamma_k)}\right)^2, \quad (3.9)$$

where $y=\alpha ZW_e/(p_ec)$ and $\Gamma(z)$ is the usual gamma function. This definition is equal to $(k+\gamma_k)F_{k-1}/(2k)$ in the notation of [31].

[1] In [31] these are called "form factor coefficients".

ΔJ	$\pi_i\pi_f$	name	relevant form factors
0 or 1	$+1$	allowed	${}^{V}F^{(0)}_{000}$, ${}^{A}F^{(0)}_{011}$
0 or 1	-1	1st forbidden non-unique	${}^{V}F^{(0)}_{101}$, ${}^{V}F^{(0)}_{110}$, ${}^{A}F^{(0)}_{111}$, ${}^{A}F^{(0)}_{211}$, ${}^{A}F^{(0)}_{000}$, ${}^{A}F^{(0)}_{011}$, ${}^{V}F^{(0)}_{101}(k_e,1,1,1)$, ${}^{A}F^{(0)}_{110}(k_e,1,1,1)$, ${}^{A}F^{(0)}_{111}(k_e,1,1,1)$
2	-1	1st forbidden unique	${}^{A}F^{(0)}_{211}$
2	$+1$	2nd forbidden non-unique	${}^{V}F^{(0)}_{211}$, ${}^{V}F^{(0)}_{220}$, ${}^{A}F^{(0)}_{221}$, ${}^{A}F^{(0)}_{321}$, ${}^{V}F^{(0)}_{220}(k_e,1,1,1)$, ${}^{A}F^{(0)}_{221}(k_e,1,1,1)$
3	$+1$	2nd forbidden unique	${}^{A}F^{(0)}_{321}$
3	-1	3rd forbidden non-unique	${}^{V}F^{(0)}_{321}$, ${}^{V}F^{(0)}_{330}$, ${}^{A}F^{(0)}_{331}$, ${}^{A}F^{(0)}_{431}$, ${}^{V}F^{(0)}_{330}(k_e,1,1,1)$, ${}^{A}F^{(0)}_{331}(k_e,1,1,1)$
4	-1	3rd forbidden unique	${}^{A}F^{(0)}_{431}$
$\vdots$	$\vdots$	$\vdots$	$\vdots$
K	$(-1)^K$	Kth forbidden non-unique	${}^{V}F^{(0)}_{K,K-1,1}$, ${}^{V}F^{(0)}_{KK0}$, ${}^{A}F^{(0)}_{KK1}$, ${}^{A}F^{(0)}_{K+1,K,1}$, ${}^{V}F^{(0)}_{KK0}(k_e,1,1,1)$, ${}^{A}F^{(0)}_{KK1}(k_e,1,1,1)$
$K+1$	$(-1)^K$	Kth forbidden unique	${}^{A}F^{(0)}_{K+1,K,1}$

Table 3.1: Classification scheme for beta decay.

The order-of-magnitude considerations of the form factors, discussed in [31], imply that the most important form factors are those presented in Table 3.1. The other form factors are suppressed by additional powers of $WR/\hbar c$, $pR/\hbar$ or $\alpha Z m_e c R/\hbar$, or they are linked to the small components of the relativistic wave function. This yields the tabulated classification scheme for beta decays: Knowing only the difference in the angular momentum and parity of the initial and final state one can see which form factors are needed and, furthermore, to which range the $\log ft$ value of the decay roughly falls.

The form factors ${}^{V/A}F^{(0)}_{KLS}$ can be associated with the nuclear matrix elements as described in [31] using the *impulse approximation*. This means that the decaying nucleon is assumed to behave like a free nucleon at the moment of the decay with all the other nucleons acting only as spectators. Then the nuclear matrix elements can be related to the form factors simply as

$$R^L\, {}^{V}F^{(0)}_{KLS} = (-1)^{K-L} g_V\, {}^{V}\mathcal{M}^{(0)}_{KLS} \tag{3.10}$$

and

$$R^L\, {}^{A}F^{(0)}_{KLS} = (-1)^{K-L+1} g_A\, {}^{A}\mathcal{M}^{(0)}_{KLS}. \tag{3.11}$$

An important additional simplification occurs in the case that the angular momentum change is $K+1$ and the product of initial and final state parities is $(-1)^K$: Then there

is only one relevant form factor to consider, and in fact all but one of the relevant nuclear matrix elements, $M = {}^{A}\mathcal{M}^{(0)}_{K+1,K,1}$, are trivially zero, and the formalism is dramatically simplified. Such decays are called *unique* decays, and for them the half-life can be expressed in the simple form

$$T_{1/2} = \frac{1}{M^2 f_K(W_0, Z, R)}, \tag{3.12}$$

where the factor

$$\begin{aligned} f_K(W_0, Z, R) = {} & \frac{g_{\mathrm{A}}^2}{\kappa(\hbar c)^{2K}(m_e c)^5} \frac{(2K)!!}{(2K+1)!!} \int_{m_e c^2}^{W_0} dW_e \, p_e c \, W_e \\ & \times \sum_{k_e+k_\nu=K+2} F_{k_e-1}(Z, W_e) \frac{[W_e^2 - (m_e c^2)^2]^{k_e-1} (W_0 - W_e)^{2k_\nu}}{(2k_e-1)!(2k_\nu-1)!} \end{aligned} \tag{3.13}$$

has no other dependence on the nucleus than the Q value, the charge and the nuclear radius.

In this work, the formalism was used in a streamlined form published in [40]. In the included publications the following shorthand notation for the nuclear matrix elements relevant to the non-unique transitions was adopted:

$$M_1 = {}^{V}\mathcal{M}^{(0)}_{K,K-1,1}, \tag{3.14a}$$
$$M_2 = {}^{V}\mathcal{M}^{(0)}_{KK0}, \tag{3.14b}$$
$$M_2^{(k_e)} = {}^{V}\mathcal{M}^{(0)}_{KK0}(k_e, 1, 1, 1), \tag{3.14c}$$
$$M_3 = {}^{A}\mathcal{M}^{(0)}_{KK1}, \tag{3.14d}$$
$$M_3^{(k_e)} = {}^{A}\mathcal{M}^{(0)}_{KK1}(k_e, 1, 1, 1), \tag{3.14e}$$
$$M_4 = {}^{A}\mathcal{M}^{(0)}_{K+1,K,1}, \tag{3.14f}$$
$$M_5 = {}^{A}\mathcal{M}^{(0)}_{000}, \tag{3.14g}$$
$$M_6 = {}^{A}\mathcal{M}^{(0)}_{011} \text{ and} \tag{3.14h}$$
$$M_6^{(k_e)} = {}^{A}\mathcal{M}^{(0)}_{011}(k_e, 1, 1, 1). \tag{3.14i}$$

3.3 Nuclear matrix elements in the adopted models

To relate the nuclear matrix elements ${}^{V/A}\mathcal{M}^{(0)}_{KLS}$ to the nuclear wave functions, it is practical to decompose them (for β^- decay) as

$${}^{V/A}\mathcal{M}^{(0)}_{KLS} = \frac{\sqrt{4\pi}}{\widehat{J}_i} \sum_{pn} {}^{V/A}m_{KLS}(pn) \, (\psi_f \| [c_p^\dagger \tilde{c}_n]_K \| \psi_i), \tag{3.15}$$

where the reduced single-particle matrix elements ${}^{V/A}m_{KLS}(pn)$ are

$$ {}^{V}m_{KLS}(pn) = \widehat{K}^{-1}(\bar{p}\|T_{KLS}\|n) \tag{3.16}$$

and

$$ {}^{A}m_{KLS}(pn) = \widehat{K}^{-1}(\bar{p}\|\gamma_5 T_{KLS}\|n). \tag{3.17}$$

The spherical components of the operator T_{KLS} are

$$ T_{KLSM} = \begin{cases} i^L r^L Y_{LM}\delta_{KL}, & S=0 \\ i^L(-1)^{L+1-K} r^L [Y_L \vec{\sigma}]_{KM}, & S=1. \end{cases} \tag{3.18}$$

The reduced single-particle matrix elements can be evaluated by taking the large components $G_{nljm}(\vec{r})$ of the single-particle wave functions

$$ \phi_{nljm}(\vec{r}) = \begin{pmatrix} G_{nljm}(\vec{r}) \\ F_{nljm}(\vec{r}) \end{pmatrix} \tag{3.19}$$

to be solutions of the non-relativistic Schrödinger equation for the harmonic oscillator. The details of this procedure and the resulting rather complex formulas can be found in [40].

The charge-changing transition densities (CCTDs) $(\psi_f\|[c_p^\dagger \tilde{c}_n]_K\|\psi_i)$ depend on the applied nuclear model. For the pnQRPA, explicit expressions can be found in [15], and for the MQPM in [8]. The formulas for evaluating the CCTDs for the pnMQPM wave functions, derived as part of this thesis work, are presented in Appendix B.

4 Applications to rare beta decays

Most of the observed beta decays are allowed, first-forbidden or second-forbidden decays with MeV-scale Q values. In this work we have studied a few selected cases of rare beta decays with an exceptionally high degree of forbiddenness or an ultra-low Q value.

The highly-forbidden non-unique beta decays have been observed in only a few isotopes: ^{113}Cd decays exclusively via a fourth-forbidden non-unique beta minus decay. ^{115}In has a recently-discovered tiny alternative decay channel with a record-low Q value discussed in detail later in this chapter. For ^{50}V only fourth-forbidden non-unique electron capture and β^- decays to excited states in the neighboring isobars have been observed, but the sixth-forbidden non-unique decays directly to their ground states are energetically possible. In ^{48}Ca and ^{96}Zr highly-forbidden beta decays compete with double beta decay. The case of ^{48}Ca has been investigated with the nuclear shell model in [41] and [42], but the beta decays of ^{113}Cd, ^{115}In and ^{96}Zr were theoretically unexplored before the work presented in this thesis.

The decays with low Q values have raised interest because of their possible use in detecting the neutrino mass by observing the shape of the beta spectrum near its end point. So far the most successful ones of such experiments have been conducted with tritium [43] yielding only an upper limit. The effort still continues e.g. in the future KATRIN[1] experiment in Karlsruhe, Germany.

4.1 Fourth-forbidden non-unique beta decays of ^{113}Cd and ^{115}In

The isotopes ^{113}Cd and ^{115}In share the unique feature that they both have a fourth-forbidden non-unique beta decay as their only decay channel, if the tiny ultra-low-Q-value decay channel of ^{115}In with an extremely low branching ratio is neglected (Figure 4.1). Even though the theory for describing such decays has been ready and experimental data has been available for decades, our calculation applying the MQPM [40] was the first theoretical calculation for the half-lives and beta spectra of these nuclei. Later we recalculated these decays as the first application for the pnMQPM

[1] Abbreviation of "KArlsruhe TRItium Neutrino experiment".

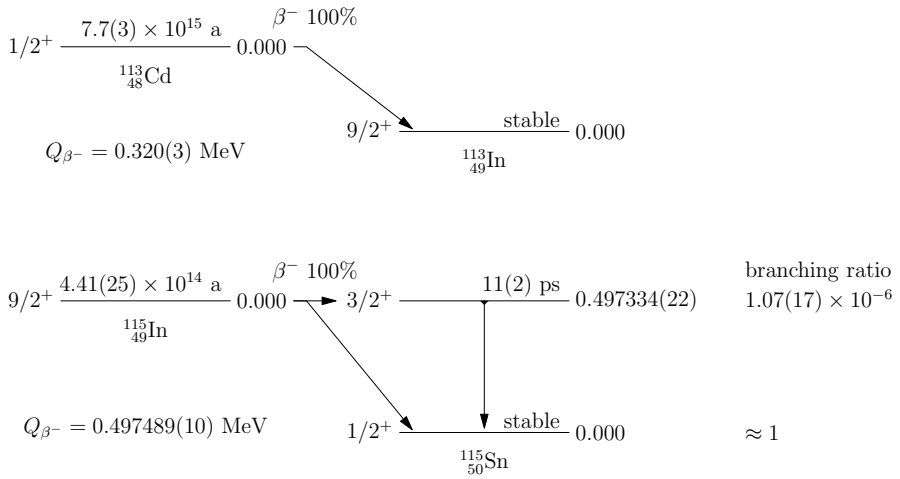

Figure 4.1: Decay scheme for ^{113}Cd and ^{115}In. The data is compiled from Refs. [18, 20, 46, 47].

[44]. The nucleus ^{115}In is interesting also due to the possibility of applying its inverse beta decay for detecting solar neutrinos. This was first suggested in [45] and has been considered to be used in the LENS[2] project [1].

The adopted valence space for our computations is illustrated in Figure 4.2. Both the initial and final state wave functions were dominantly of one-quasiparticle nature both in the MQPM and pnMQPM results, which was to be expected considering that they are ground states of the respective odd-mass nuclei. The low-energy spectra were reproduced reasonably well with both models with the exception of the ^{113}Cd pnMQPM spectrum, in which the dominantly three-quasiparticle states remained notably higher in energy than their experimental counterparts. When compared to the experimental data (Figure 4.3), the ^{113}Cd half-life seemed to notably improve when moving from the MQPM to the pnMQPM description. For ^{115}In, there did not seem to be much improvement.

The situation got more interesting as the effect of the Q value was investigated closer. We calculated the theoretical half-lives published in [40] and [44] and presented in Figure 4.3 with the Q values taken from Nuclear Data Sheets [18, 20]. However, the half-life has a strong dependence on the Q value and the agreement on the Q value between different experiments is not as good as on the half-life. The Q value dependence of the theoretical half-life is presented in Figures 4.4 and 4.5 along with the results of only those of the experiments that yielded both half-life and Q value.

For ^{113}Cd all but the latest one of these experiments agree better with the pnMQPM than with the MQPM result. Unfortunately, no ion-trap precision measurement for

[2]Abbreviation of "Low Energy Neutrino Spectroscopy".

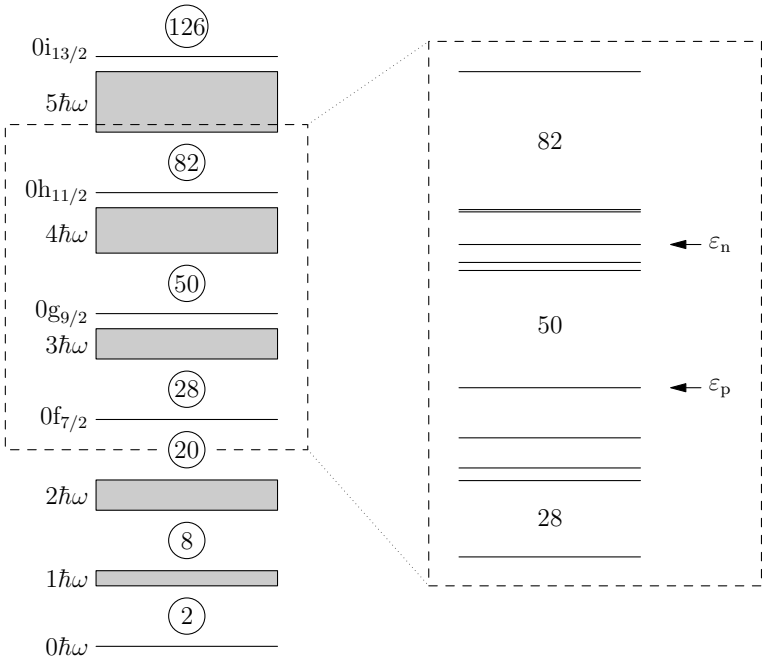

Figure 4.2: Schematic illustration of the chosen valence space for the ^{113}Cd and ^{115}In calculations. Approximate locations of the Fermi levels are indicated with ε_n and ε_p for neutrons and protons respectively.

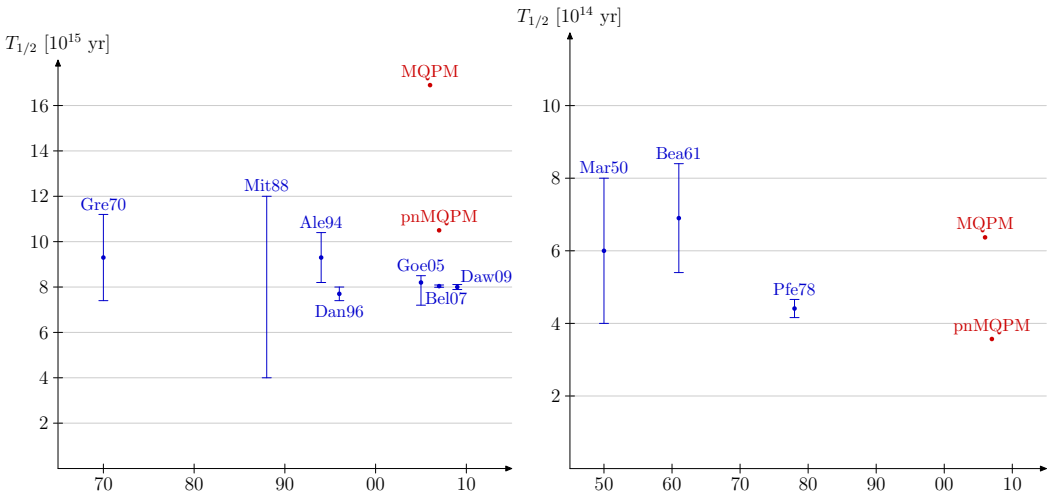

Figure 4.3: Collected half-life measurements and calculations for both ^{113}Cd (left) and ^{115}In (right). The horizontal axis shows the year of publication, illustrating the development of experimental techniques. The experimental values are from [48] (Gre70), [49] (Mit88), [50, 51] (Ale94), [52] (Dan96), [3] (Goe05), [53] (Bel07) and [54] (Daw09) for cadmium and from [55] (Mar50), [56] (Bea61) and [57] (Pfe78) for indium.

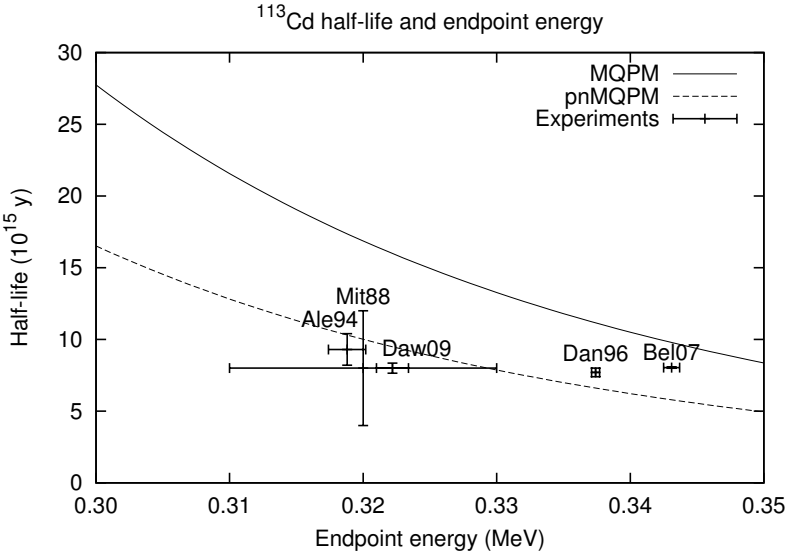

Figure 4.4: Calculated ^{113}Cd half-life as a function of the decay Q value. The experimental measurements are from [49] (Mit88), [50, 51] (Ale94), [52] (Dan96), [53] (Bel07) and [54] (Daw09).

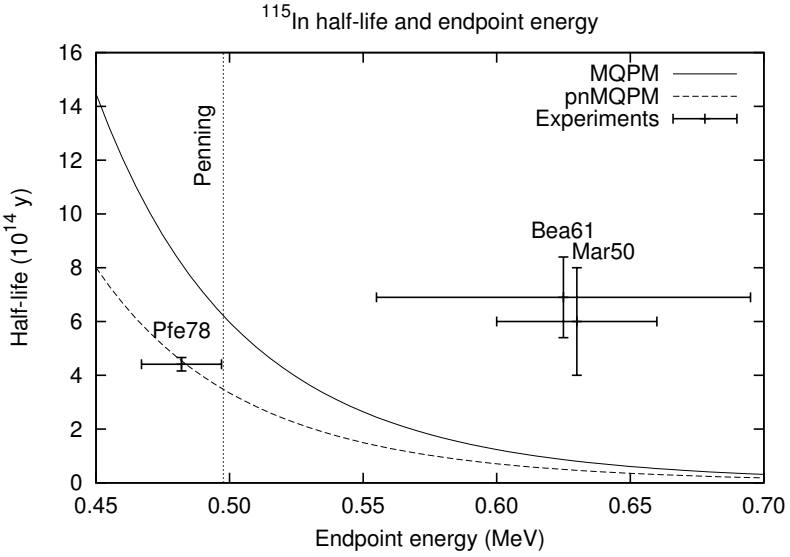

Figure 4.5: Calculated ^{115}In half-life as a function of the decay Q value. The experimental values are from [55] (Mar50), [56] (Bea61) and [57, 58] (Pfe78). The vertical dotted line represents the Penning-trap measurements [46, 47] for the Q value. Their difference and their error bars are smaller than the line thickness.

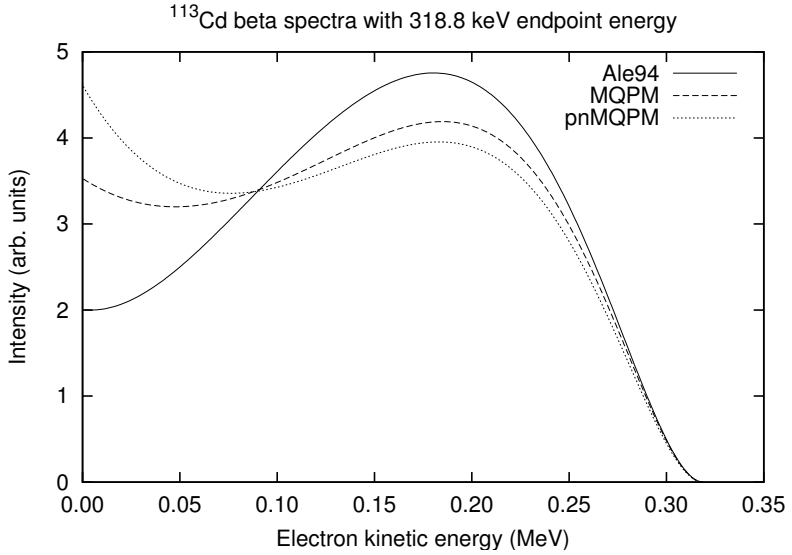

Figure 4.6: Calculated MQPM and pnMQPM beta spectra compared to the experimental one from [50] for ^{113}Cd. Previously published in [59].

the Q value has been published to date. In the case of ^{115}In the pnMQPM result agrees perfectly with the latest experiment (labeled Pfe78), which in turn had a notably different Q value than the previous measurements. The two fresh Penning trap experiments [46, 47] agree with Pfe78.

The experiments for the highly-forbidden beta decays are very demanding, because the half-lives are comparable to those of double beta decays. While all the different half-life measurements agree very well with each other (Figure 4.3), the beta spectrum shape especially on the low-energy end has been more challenging to determine experimentally. This can be seen clearly by comparing the three measured spectrum shapes for ^{113}Cd (Figures 4.6, 4.7, 4.8 and 4.9). In each figure, the theoretical MQPM and pnMQPM spectra have been calculated using the Q value obtained from the corresponding experiment.

Both experimental and theoretical spectra share the feature of a "hill". In the theoretical spectra this hill is located at approximately 0.2 MeV, and in the experimental spectra around 0.15 MeV [52, 53, 54] or 0.2 MeV [50]. The low-energy behavior of the theoretical spectra cannot be accessed in the measurements since the experiments are inaccurate at low electron energies. The experimental spectra differ significantly from each other on the low-energy region since they have different statistics and the extrapolation procedure adopted is questionable.

The shape factor used in the fitted function for the experimental beta spectra of ^{113}Cd is the one suited for the third-forbidden unique decay [60]. While this choice

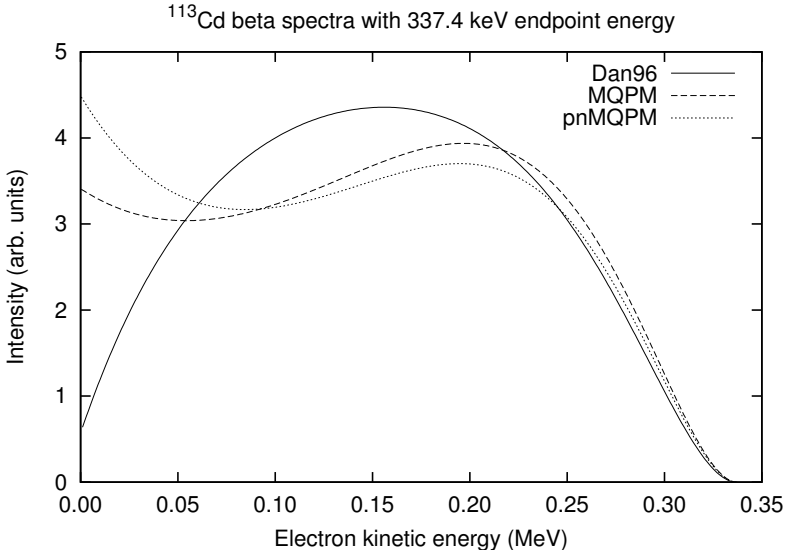

Figure 4.7: Calculated MQPM and pnMQPM beta spectra compared to the experimental one from [52] for ^{113}Cd. Previously published in [59].

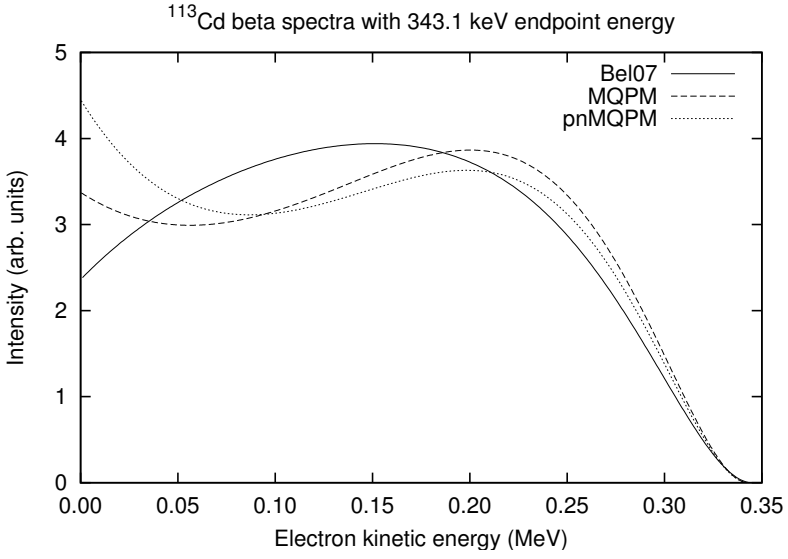

Figure 4.8: Calculated MQPM and pnMQPM beta spectra compared to the experimental one from [53] for ^{113}Cd. Previously published in [59].

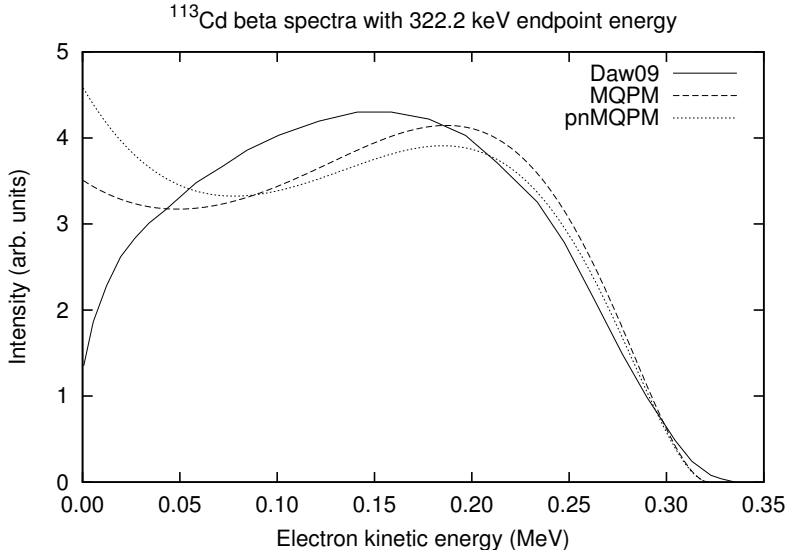

Figure 4.9: Calculated MQPM and pnMQPM beta spectra compared to the experimental one from [54] for ^{113}Cd.

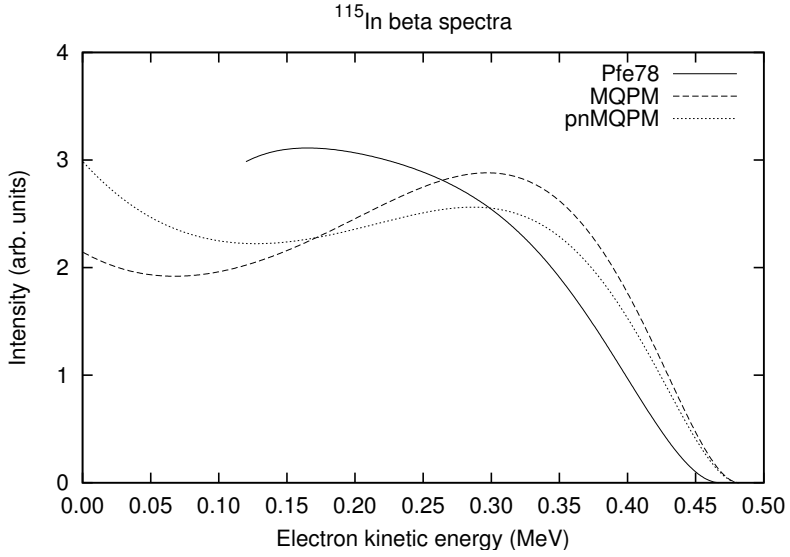

Figure 4.10: Calculated MQPM and pnMQPM beta spectra compared to the experimental one from [57] for ^{115}In. Previously published in [59].

is dubious, it seems to work reasonably well in the high-energy end of the spectrum. Since the uncertainties in the measurements are significantly larger in the low-energy end of the spectrum, the parameters of the fit are more sensitive to the details of the high-energy spectrum, resulting in the differences between the experiments seen in the low-energy region. Unfortunately, no simple fittable function with a reasonably small number of parameters is available for the non-unique case. Due to the dubious shape factor used in the experimental fits and the very different statistics on the low-energy region in different experiments, no definite conclusions can be drawn from the presently available data.

For ^{115}In there is only one existing measurement for the spectrum shape [57] (Figure 4.10). The experimental spectrum hints to the existence of a hill around 0.2 MeV, whereas the calculations put the hill near 0.3 MeV. The spectrum shape for the region below 0.1 MeV is completely unknown. The lack of more precise data makes the comparison of the spectra ambiguous.

4.2 Single-beta decay channels of ^{96}Zr

The zirconium isotope ^{96}Zr decays primarily via double beta decay [61]. Although the single beta decay for this isotope is not yet experimentally observed, it is energetically allowed and hence competes with the double beta decay (See Figure 4.11). The experimental lower limit for the single-beta-decay half-life is 3.8×10^{19} years (90% C.L.) [62]. The single beta decay is hindered, because all the energetically allowed single-beta-decay channels are highly forbidden and the Q values of these channels are very low.

The geochemical measurements for the double-beta-decay half-life of ^{96}Zr have produced contradictory results: The experiment of Kawashima *et al.* [63], where a zircon mineral sample from Cable Sands, Australia, was analyzed to determine the excess amount of ^{96}Mo, yielded the half-life of $(3.9 \pm 0.9) \times 10^{19}$ years. However, a similar experiment by Wieser *et al.* [64] on a zircon mineral from the same geographical region resulted in a significantly shorter estimate, $(9.4 \pm 3.2) \times 10^{18}$ years.

In addition to the geochemical experiments, the double-beta-decay half-life has also been measured in the NEMO-2 [65] and NEMO-3 experiments [66]. Their results, $(2.1^{+0.8(\mathrm{stat.})}_{-0.4(\mathrm{stat.})} \pm 0.2(\mathrm{syst.})) \times 10^{19}$ y and $(2.35 \pm 0.14(\mathrm{stat.}) \pm 0.16(\mathrm{syst.})) \times 10^{19}$ y respectively, are in perfect agreement with each other but disagree with both of the geochemical measurements.

The aim of our calculation [67] for the half-lives of the single-beta-decay channels was to estimate the possible contamination for the geochemical double-beta-decay half-

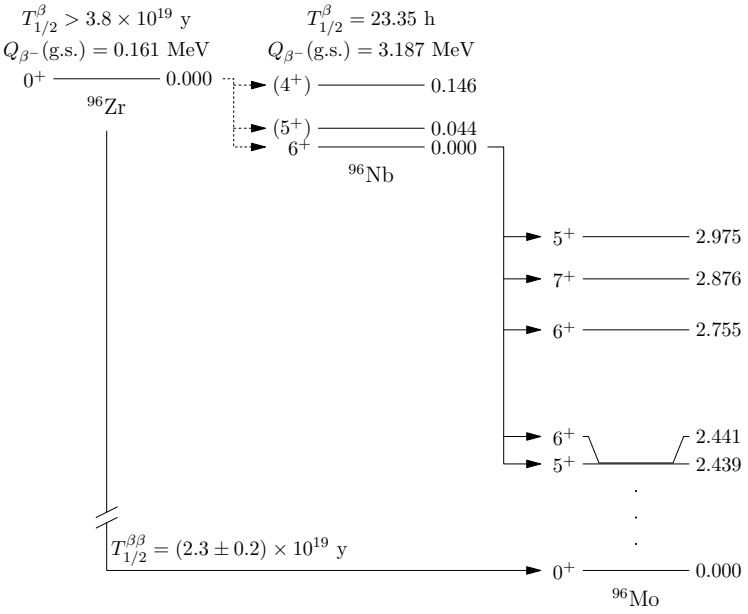

Figure 4.11: Decay scheme of ^{96}Zr. The dotted decay channels have not yet been experimentally observed. The data on this figure is compiled from [62], [68] and [69]. Originally published in [70].

life measurements. As seen in Figure 4.11, the single beta decay of ^{96}Zr is followed by another beta decay to ^{96}Mo with a negligible time scale compared to the ^{96}Zr lifetime, and it is impossible to know if a ^{96}Mo atom in a geological sample has been produced via a double beta decay or two consecutive single beta decays.

In our calculation the valence space for both protons and neutrons consisted of 15 states reaching from the $3\hbar\omega$ to the $5\hbar\omega$ oscillator major shell (Figure 4.12). The procedure for describing the ^{96}Nb daughter nucleus using the pnQRPA is described in Chapter 2. The interaction was unscaled in the pnQRPA calculation, i.e. the bare values $g_{\text{ph}} = g_{\text{pp}} = 1$ were used for each multipolarity in the pnQRPA.

Our calculated results for the partial half-lives imply that the decay channel to the 5^+ excited state clearly dominates in the single-beta decay. According to our results, the decay to the 6^+ ground state is completely negligible and the decay to the 4^+ state only contributes a couple per cent. The total computed half-life, 2.4×10^{20} y, is roughly an order of magnitude longer than the current experimental lower limit, hinting that this beta decay half-life might be reachable in near-future experiments. In [70], we have recomputed the half-lives using newer Q values, but the updated results are close to the ones published in [67] and the conclusions are not affected.

The calculated single-beta-decay half-life is well within the error bars of both of the geochemical experiments. Therefore correcting for the beta-decay contamination is not crucial before more accurate geochemical data becomes available, especially since

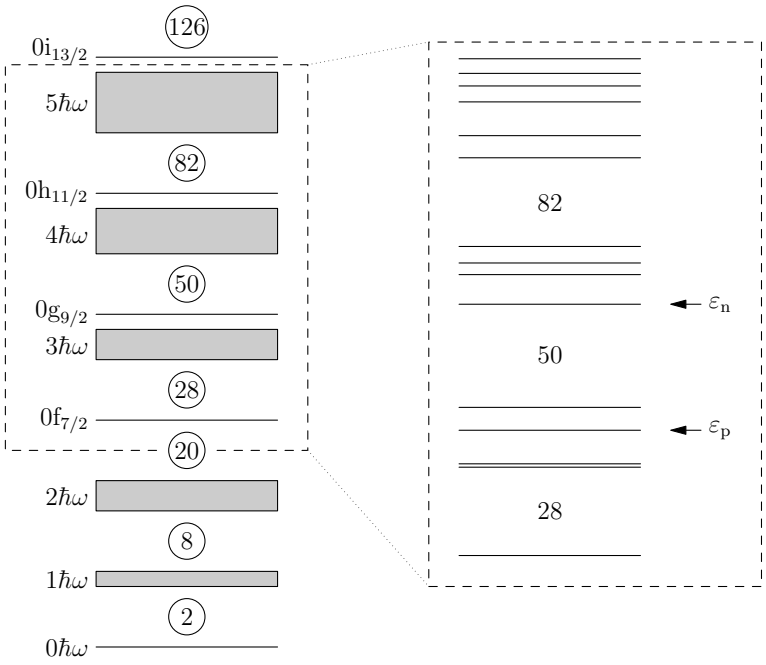

Figure 4.12: Schematic illustration of the chosen valence space for the ^{96}Zr calculation. Approximate locations of the Fermi levels are indicated.

the disagreement with each other and the NEMO experiments remains an unanswered question for the geochemical experiments on ^{96}Zr.

4.3 Ultra-low-Q-value decay of ^{115}In

The beta decay of ^{115}In to the first excited state of ^{115}Sn (see Figure 4.1) was first observed by Cattadori *et al.* [71]. They recognized it to possibly have the lowest observed Q value and hence suggested the possibility of using this decay as an independent probe for the neutrino mass. The existence of this decay channel was confirmed and the half-life measurement refined in an experiment conducted in the HADES underground laboratory in Belgium [46].

In Penning trap measurements conducted by the JYFLTRAP group in the Department of Physics at the University of Jyväskylä the Q value of this decay was discovered to be (0.35 ± 0.17) keV, roughly an order of magnitude lower than the previous record [46]. The Q value was further refined to (0.155 ± 0.024) keV by a similar independent measurement in the Florida State University [47].

The ground-state-to-excited-state transition is a second-forbidden unique beta minus

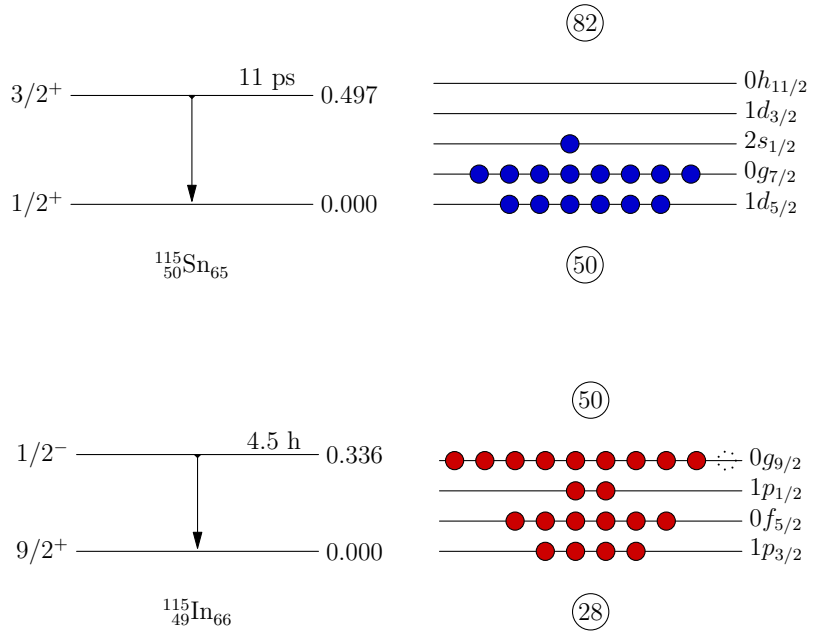

Figure 4.13: Simple one-quasiparticle interpretation for the lowest states of ^{115}In and ^{115}Sn can easily explain the observed angular momenta and parities. The first excited state of ^{115}Sn is simply the excitation of the unpaired neutron to the $1d_{3/2}$ orbit. This interpretation is also consistent with the MQPM [40] and pnMQPM [44] calculations.

decay. For unique decays all but one of the nuclear matrix elements of the general beta-decay formalism vanish, and the calculation of the decay half-life is simplified enormously: The partial half-life of this decay channel is simply inversely proportional to the square of the nuclear matrix element M (equal to M_4 in the notation of [40] and ${}^{A}\mathcal{M}^{(0)}_{K+1,K1}$ in the notation of [31]), or more formally,

$$T_{1/2} = \frac{1}{M^2 f_K(w_0, Z_f, R)}, \tag{4.1}$$

where $f_K(w_0, Z_f, R)$, given in (3.13), is the phase-space integral depending only on the end-point energy w_0, the charge of the daughter nucleus Z_f and the nuclear radius R, but not the details of the nuclear wave functions.

We used the pnMQPM to calculate the initial and final nuclear wave functions using the same values for the adjustable parameters as in our earlier work for the ground-state-to-ground-state decay channel [44]. The composition of both the initial and final state wave function implies that these both states are dominantly one-quasiparticle states. This interpretation is consistent with the naïve one-particle/one-hole description depicted in Figure 4.13.

Unexpectedly, the computed half-life as the function of the Q value (Figure 4.14) has a significant disagreement with the experimental results. As the pnMQPM description

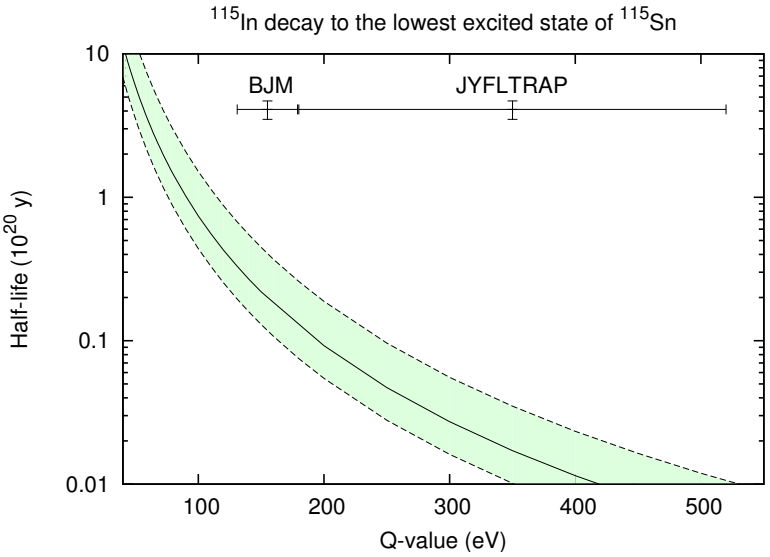

Figure 4.14: Computed partial half-life of the ^{115}Sn excited-state transition as a function of the Q value. The green band represents an *ad hoc* 30% uncertainty in the nuclear matrix element, giving a visual clue of how unsensitive the curve is to the uncertainties in the nuclear description. This figure was published in [72].

reproduces the ground-state-to-ground-state transition half-life rather accurately, it is reasonable to expect a similar agreement here. However, to reach the 1σ limits of the most accurate measurement available (the HADES half-life measurement [46] combined with the Florida State University Q value measurement [47]) the theoretical half-life curve would have to be multiplied by roughly a factor of 15. If this difference was solely due to the inaccuracy of the nuclear matrix element, it would have to be off by roughly a factor of 4. An error that large requires that either our interpretation of the simple structure of the final state is wrong or we are missing a crucial piece of the puzzle.

While we cannot rule out the possibility that the discrepancy between the theoretical prediction and the experimental data would not be due to a more exotic configuration of the final state, there is another possible explanation for it. There are several little-studied effects stemming from atomic electrons: The electron screening, the atomic overlap effect, the exchange effects and the final-state interactions. While these effects are negligible for the beta decays studied before this one, the fact that we are now on a new record-low-Q-value regime motivated us to take a closer look at them.

The electron screening corrections are traditionally estimated using the Rose prescription [37]. There also exists a more refined formula for taking them into account, namely the completely relativistic expression by Lopez and Durand [73]. Neither of these approximations is applicable to the ultra-low Q values: For the case of ^{115}In they

break down so badly that they actually yield a large negative half-life.

The atomic overlap effect is caused by the fact that the electron states of the final atom are not exactly the same as those of the initial atom. This effect was studied by Bahcall [74] for allowed decays. According to his estimates, the decay is hindered by this effect the more the lower the Q value. The case with the lowest Q value he studied was the ^{241}Pu beta decay with the Q value of 21 keV. For that decay his estimates yielded a 2% hindrance in the decay half-life. However, his method breaks down for Q values as low as a few hundred eV.

The exchange effects were also first estimated by Bahcall in [74]. He concluded that these effects would cause additional reduction in the decay rate, 2% in the case of ^{241}Pu. However, the theoretical effort by Harston and Pyper [75] contradicts his estimates, concluding that the exchange effects may actually *enhance* the decay. Their calculation yielded a 7.5% enhancement on the ^{241}Pu decay rate.

The molecular *final-state interactions* have only been studied for the beta decay of tritium [76]. In case of ^{115}In the role of final-state interactions in the lattice is a completely uninvestigated territory: We do not know if the chemical bonds of the indium atoms in the sample introduce any non-negligible corrections to the ultra-low-Q-value decay.

It should be emphasized that even if the discrepancy did turn out to be due to an incorrect interpretation of the final state, the fact that the atomic contributions are not investigated for energies this low remains. Now that the advancements in experimental techniques have made it possible to access such extreme Q values, the theory should be extended to cover this region as well.

The nuclear theory community seems to have lost interest in the atomic effects after the early studies showed them to be negligible for the usual beta-decay Q values. An exception for this has been the tritium beta decay, which has been used as a tool in search for the neutrino mass (e.g. [43]), and where the atomic cloud is extraordinarily simple having only one electron. Now that the experimental techniques have been developed far enough to access decays where the old approximations break down, new theoretical work is needed to fill this gap in beta-decay theory. However, finding other likely candidates for observing an ultra-low-Q-value decay is currently difficult due to the fact that the atomic masses (or the ground-state-to-ground-state beta-decay Q values) are not yet systematically measured with sufficient accuracy, not even in the valley of beta stability.

Experimental verification of the atomic contributions to beta decays is not possible at the moment either, because the uncertainties in the nuclear wave functions are still so large that the small corrections are dwarfed by their presence. Therefore properly closing all the open questions presented here may have to wait until the nuclear struc-

ture theory has advanced considerably. Still, theoretical estimates for the magnitude of the atomic contributions for the ultra-low-Q-value beta decays can be done. If they turn out to be large enough and if other experimentally observable cases were found, it might be possible to verify their existence experimentally.

5 Summary

In this thesis several rare beta decays were investigated using theoretical nuclear-structure and decay tools. These decays were the highly-forbidden non-unique beta decays of ^{113}Cd and ^{115}In, the single-beta-decay channels of ^{96}Zr and the recently discovered ultra-low-Q-value decay channel of ^{115}In.

As part of the project the proton-neutron microscopic quasiparticle-phonon model (pnMQPM) was developed. Its application to the ground-state-to-ground-state decays of ^{113}Cd and ^{115}In was successful. The advantages of the pnMQPM over MQPM are that one can use partly different set of experimental data to fine-tune the model parameters and that the pnQRPA fulfills the Ikeda sum rule, possibly improving the beta-decay calculations.

The primary weakness of the pnMQPM model is that its configuration space does not include the three-proton or three-neutron degrees of freedom. For some states these degrees of freedom are important and the pnMQPM wave functions are inevitably more inaccurate than the MQPM ones. This is a severe limitation of the pnMQPM. However, on the applications presented in this thesis, these contributions were not significant, since the initial and final states of the studied decays of the odd-mass nuclei were dominantly one-quasiparticle states.

When studying the wave function composition of the low-energy three-quasiparticle states, we also observed that in the MQPM picture there usually is one dominant configuration (a quasiparticle coupled to a QRPA phonon), but in the pnMQPM there are often four or five equally strong major configurations (a quasiparticle coupled to a pnQRPA excitation). In this sense, the MQPM approach is a more natural way of describing the structure of the wave functions.

The half-lives of the fourth-forbidden non-unique ground-state-to-ground-state beta decays of ^{113}Cd and ^{115}In were slightly better estimated using the pnMQPM than the MQPM approach, although a large difference was not to be expected, since all the involved states had only small three-quasiparticle components in both models. The beta spectra were very similar, and the experimental data is not accurate enough to favor one model over another in this respect.

Our investigation of the ^{96}Zr single-beta-decay channels using the pnQRPA approach yielded a half-life estimate of 2.4×10^{20} y. This value is roughly an order of magnitude

longer that the current experimental lower limit for the single beta decay and well within the uncertainties of the geochemical results for the double-beta-decay half-life. Therefore the contamination from the single-beta-decay channels on the geochemical experiments can presently be neglected.

Our calculation on the ^{115}In second-forbidden unique beta decay to the first excited state of ^{115}Sn using the pnMQPM approach is off by roughly a factor of 15. Because the decay is unique, the dependence of the half-life on the nuclear wave functions is extraordinarily simple, and the inaccuracy of the model cannot explain the discrepancy unless our interpretation of the dominantly one-quasiparticle structure of the final state is completely wrong.

The Q value of this decay is measured to be significantly lower than any beta-decay Q value observed before, about an order of magnitude smaller than that of ^{187}Re. This motivated us to consider an alternative explanation for the discrepancy: the atomic effects, namely the electron screening, the exchange and overlap effects and the molecular final-state interactions. Reviewing the literature on these effects revealed that the research on them is not directly applicable to this decay, but there is a clear trend that they grow more and more important as the Q value decreases. These effects deserve to be studied more carefully.

References

[1] C. Grieb. Nucl. Phys. B: Proc. Suppl. **168** (2007) 122.

[2] K. Zuber. Phys. Lett. B **519** (2001) 1.

[3] C. Goessling *et al.* Phys. Rev. C **72** (2005) 064328.

[4] NuDat 2 database. `http://www.nndc.bnl.gov/nudat2/`.

[5] V. G. Soloviev. *Theory of atomic nuclei: quasiparticles and phonons* (IOP Publishing, Bristol, 1992).

[6] D. S. Delion and J. Suhonen. Phys. Rev. C **67** (2003) 034301.

[7] D. S. Delion and J. Suhonen. Nucl. Phys. A **781** (2007) 88.

[8] J. Toivanen and J. Suhonen. Phys. Rev. C **57** (1998) 1237.

[9] A. Bohr and B. R. Mottelson. *Nuclear Structure*, volume I (W. A. Benjamin, New York, 1969).

[10] J. Bardeen, L. N. Cooper and J. R. Schrieffer. Phys. Rev. **108** (1957) 1175.

[11] A. Bohr, B. R. Mottelson and D. Pines. Phys. Rev. **110** (1958) 936.

[12] N. N. Bogoliubov. Sov. Phys. JETP **7** (1958) 41.

[13] J. G. Valatin. Phys. Rev. **122** (1961) 1012.

[14] M. Baranger. Phys. Rev. **120** (1960) 957.

[15] J. Suhonen. *From Nucleons to Nucleus: Concepts of Microscopic Nuclear Theory* (Springer, Berlin, 2007).

[16] K. Holinde. Phys. Rep. **68** (1981) 121.

[17] D. de Frenne and E. Jacobs. Nucl. Data Sheets **79** (1996) 639.

[18] J. Blachot. Nucl. Data Sheets **104** (2005) 791.

[19] J. Blachot. Nucl. Data Sheets **97** (2002) 593.

[20] J. Blachot. Nucl. Data Sheets **104** (2005) 967.

[21] J. Blachot. Nucl. Data Sheets **92** (2001) 455.

[22] K. L. G. Heyde. *The nuclear shell model* (Springer, Berlin, 1994), 2nd edition.

[23] J. A. Halbleib, Sr. and R. A. Sorensen. Nucl. Phys. A **98** (1967) 542.

[24] D. J. Rowe. Rev. Mod. Phys. **40** (1968) 153.

[25] N. Ullah and D. J. Rowe. Nucl. Phys. A **163** (1971) 257.

[26] K. Ikeda. Prog. Theor. Phys. **31** (1964) 434.

[27] J. Toivanen and J. Suhonen. J. Phys. G: Nucl. Part. Phys. **21** (1995) 1491.

[28] J. Suhonen *et al.* Nucl. Phys. A **628** (1998) 41.

[29] B. Singh, A. A. Rodionov and Y. L. Khazov. Nucl. Data Sheets **109** (2008) 517.

[30] D. J. Rowe. J. Math. Phys. **10** (1969) 1774.

[31] H. Behrens and W. Bühring. *Electron radial wave functions and nuclear beta decay* (Clarendon, Oxford, 1982).

[32] E. Fermi. Z. Phys. **88** (1934) 161.

[33] G. Gamow and E. Teller. Phys. Rev. **149** (1936) 895.

[34] C. S. Wu, E. Ambler, R. W. Hayward, D. D. Hoppes and R. P. Hudson. Phys. Rev. **105** (1957) 1413.

[35] M. E. Peskin and D. V. Schroeder. *An Introduction to Quantum Field Theory* (Perseus Books, Cambridge, Massachusetts, 1995).

[36] F. Halzen and A. D. Martin. *Quarks and leptons: An introductory course in modern particle physics* (Wiley, New York, 1984).

[37] M. E. Rose. Phys. Rev. **49** (1936) 727.

[38] J. J. Matese and W. R. Johnson. Phys. Rev. **150** (1966) 846.

[39] J. C. Hardy, I. S. Towner, V. T. Koslowsky, E. Hagberg and H. Schmeing. Nucl. Phys. A **509** (1990) 429.

[40] M. T. Mustonen, M. Aunola and J. Suhonen. Phys. Rev. C **73** (2006) 054301. Included in this thesis. Erratum Phys. Rev. C **76** (2007) 019901(E).

[41] E. K. Warburton. Phys. Rev. C **31** (1985) 1896.

[42] M. Aunola, J. Suhonen and T. Siiskonen. Europhys. Lett. **46** (1999) 577.

[43] C. Kraus *et al.* Eur. Phys. J. C **40** (2005) 447.

[44] M. T. Mustonen and J. Suhonen. Phys. Lett. B **657** (2007) 38. Included in this thesis.

[45] R. S. Raghavan. Phys. Rev. Lett. **37** (1976) 259.

[46] J. S. E. Wieslander *et al.* Phys. Rev. Lett. **103** (2009) 122501. Included in this thesis.

[47] B. J. Mount, M. Redshaw and E. G. Myers. Phys. Rev. Lett. **103** (2009) 122502.

[48] W. E. Greth, S. Gangadharan and R. L. Wolke. J. Inorg. Nucl. Chem. **32** (1970) 2113.

[49] L. W. Mitchell and P. H. Fisher. Phys. Rev. C **38** (1988) 895.

[50] A. Alessandrello *et al.* Nucl. Phys. B Proc. Suppl. **35** (1994) 394.

[51] A. Alessandrello *et al.* Nucl. Instrum. Methods A **344** (1994) 243.

[52] F. A. Danevich *et al.* Phys. Atom. Nucl. **59** (1996) 1.

[53] P. Belli *et al.* Phys. Rev. C **76** (2007) 064603.

[54] J. V. Dawson *et al.* Nucl. Phys. A **818** (2009) 264.

[55] E. A. Martell and W. F. Libby. Phys. Rev. **80** (1950) 977.

[56] G. B. Beard and W. H. Kelly. Phys. Rev. **122** (1961) 1576.

[57] L. Pfeiffer, J. Allen P. Mills, E. A. Chandross and T. Kovacs. Phys. Rev. C **19** (1978) 1035.

[58] L. Pfeiffer, J. Allen P. Mills, R. S. Raghavan and E. A. Chandross. Phys. Rev. Lett. **41** (1978) 63.

[59] M. T. Mustonen and J. Suhonen. Proceedings of the 2-nd International Conference "Current Problems in Nuclear Physics and Atomic Energy" (NPAE-Kyiv2008) page 493. Available online at `http://www.kinr.kiev.ua/NPAE-Kyiv2008/proceedings/`.

[60] C. S. Wu. In *Alpha-, beta- and gamma-ray spectroscopy*, volume 2 (North-Holland, Amsterdam, 1965).

[61] F. T. Avignone III, S. R. Elliott and J. Engel. Rev. Mod. Phys. **80** (2008) 481.

[62] C. Arpesella *et al.* Europhys. Lett. **27** (1994) 29.

[63] A. Kawashima, K. Takahashi and A. Masuda. Phys. Rev. C **47** (1993) R2452.

[64] M. E. Wieser and J. R. De Laeter. Phys. Rev. C **64** (2001) 024308.

[65] R. Arnold *et al.* Nucl. Phys. A **658** (1999) 299.

[66] A. S. Barabash. AIP Conf. Proc. **1180** (2009) 6.

[67] H. Heiskanen, M. T. Mustonen and J. Suhonen. J. Phys. G: Nucl. Part. Phys. **34** (2007) 837. Included in this thesis.

[68] D. Abriola and A. A. Sonzogni. Nucl. Data Sheets **109** (2008) 2501.

[69] Y. A. Shitov. Phys. Atom. Nucl. **69** (2006) 2090.

[70] M. T. Mustonen and J. Suhonen. AIP Conf. Proc. **1180** (2009) 76. Included in this thesis.

[71] C. M. Cattadori, M. De Deo, M. Laubenstein, L. Pandola and V. I. Tretyak. Nucl. Phys. A **748** (2005) 333.

[72] M. T. Mustonen and J. Suhonen. J. Phys. G: Nucl. Part. Phys. **37** (2010) 064008. Included in this thesis.

[73] J. L. Lopez and L. Durand. Phys. Rev. C **37** (1988) 535.

[74] J. N. Bahcall. Phys. Rev. **129** (1963) 2683.

[75] M. R. Harston and N. C. Pyper. Phys. Rev. A **45** (1992) 6282.

[76] A. Saenz and P. Froelich. Phys. Rev. C **56** (1997) 2132.

A Hamiltonian matrix elements for the pnMQPM

The one-quasiparticle states are eigenstates of the BCS Hamiltonian, i.e.

$$\langle\alpha|\hat{H}|\alpha'\rangle = \delta_{\alpha\alpha'}E_a \tag{A.1}$$

for both proton and neutron states. The non-trivial Hamiltonian matrix elements are the ones involving a three-quasiparticle state as an initial or final state. In the case of the proton-odd nucleus they read

$$\begin{aligned}\langle\pi|\hat{H}|\nu\omega;jm\rangle = 2\frac{\widehat{J_\omega}}{\widehat{j}}\delta_{jj_p}\delta_{mm_\pi}\sum_{p'n'}\big[&(u_{p'}u_{n'}X^\omega_{p'n'} - v_{p'}v_{n'}Y^\omega_{p'n'})u_pv_nG(pnp'n'J_\omega)\\ &-(v_{p'}v_{n'}X^\omega_{p'n'} - u_{p'}u_{n'}Y^\omega_{p'n'})v_pu_nG(pnp'n'J_\omega)\\ &+(v_{p'}u_{n'}X^\omega_{p'n'} + u_{p'}v_{n'}Y^\omega_{p'n'})v_pv_nF(pnp'n'J_\omega)\\ &-(u_{p'}v_{n'}X^\omega_{p'n'} + v_{p'}u_{n'}Y^\omega_{p'n'})u_pu_nF(pnp'n'J_\omega)\big],\end{aligned} \tag{A.2}$$

where $G(pnp'n'J_\omega)$ and $F(pnp'n'J_\omega)$ are the interaction matrix elements as defined in [14, 15], and

$$\begin{aligned}\langle\nu'\omega';jm|\hat{H}|\nu\omega;jm\rangle &= (E_n+E_\omega)\delta_{nn'}\delta_{\omega\omega'}\\ &+\widehat{J_\omega}\widehat{J_{\omega'}}\sum_p\left(\begin{Bmatrix} j_n & j_p & J_{\omega'}\\ j_{n'} & j & J_\omega\end{Bmatrix}X^{\omega'}_{pn}X^\omega_{pn'}(E_\omega+E_{\omega'}-E_p)+\frac{\delta_{jj_p}}{\widehat{j^2}}Y^{\omega'}_{pn'}Y^\omega_{pn}E_p\right),\end{aligned} \tag{A.3}$$

where the sum runs over the proton states. Correspondingly for the neutron-odd nucleus

$$\begin{aligned}\langle\nu|\hat{H}|\pi\omega;jm\rangle = 2\frac{\widehat{J_\omega}}{\widehat{j}}\delta_{jj_n}\delta_{mm_\nu}(-1)^{j_p+j_n+J_\omega+1}&\\ \times\sum_{p'n'}\big[&(u_{p'}u_{n'}X^\omega_{p'n'} - v_{p'}v_{n'}Y^\omega_{p'n'})v_pu_nG(pnp'n'J_\omega)\\ &-(v_{p'}v_{n'}X^\omega_{p'n'} - u_{p'}u_{n'}Y^\omega_{p'n'})u_pv_nG(pnp'n'J_\omega)\\ &+(u_{p'}v_{n'}X^\omega_{p'n'} + v_{p'}u_{n'}Y^\omega_{p'n'})v_pv_nF(pnp'n'J_\omega)\\ &-(v_{p'}u_{n'}X^\omega_{p'n'} + u_{p'}v_{n'}Y^\omega_{p'n'})u_pu_nF(pnp'n'J_\omega)\big]\end{aligned} \tag{A.4}$$

and

$$\left\langle \pi'\omega'; jm \middle| \hat{H} \middle| \pi\omega; jm \right\rangle = (E_p + E_\omega)\delta_{pp'}\delta_{\omega\omega'} - (-1)^{j_p+j_{p'}+J_\omega+J_{\omega'}}\widehat{J_\omega}\widehat{J_{\omega'}} \times \sum_n \left(\begin{Bmatrix} j_p & j_n & J_{\omega'} \\ j_{p'} & j & J_\omega \end{Bmatrix} X^{\omega'}_{pn} X^{\omega}_{p'n} (E_\omega + E_{\omega'} - E_n) + \frac{\delta_{jj_n}}{\widehat{j^2}} Y^{\omega'}_{p'n} Y^{\omega}_{pn} E_n \right), \quad \text{(A.5)}$$

where the sum runs over the neutron states.

B Charge-changing transition densities in the pnMQPM

In the present notation the label p (with and without a subscript) is always labeling a proton orbit and n a neutron orbit. For the β^- decay from a neutron-odd to a proton-odd nucleus, the pnMQPM charge-changing transition densities (CCTDs) are

$$(p_f\|[c_p^\dagger \tilde{c}_n]_L\|n_i) = \delta_{pp_f}\delta_{nn_i}\widehat{L}u_p u_n, \tag{B.1}$$

$$\begin{aligned}(p_f\|[c_p^\dagger \tilde{c}_n]_L\|p_i\omega_i; j_i) = (-1)^{j_{p_i}+J_{\omega_i}+j_i+1}\widehat{j_i}\Bigg[&\delta_{p_ip_f}\delta_{J_{\omega_i}L}(v_pu_nX^{\omega_i}_{pn} + u_pv_nY^{\omega_i}_{pn}) \\ &+ \widehat{J_{\omega_i}}\widehat{L}\left(\delta_{pp_i}\begin{Bmatrix} j_{p_f} & L & j_i \\ j_p & J_{\omega_i} & j_n\end{Bmatrix} v_pu_nX^{\omega_i}_{p_fn} - \delta_{pp_f}\frac{\delta_{j_ij_n}}{\widehat{j_i}^2}u_pv_nY^{\omega_i}_{p_in}\right)\Bigg],\end{aligned} \tag{B.2}$$

$$\begin{aligned}(n_f\omega_f; j_f\|[c_p^\dagger \tilde{c}_n]_L\|n_i) = \widehat{j_f}\Bigg[&\delta_{n_in_f}\delta_{J_{\omega_f}L}(u_pv_nX^{\omega_f}_{pn} + v_pu_nY^{\omega_f}_{pn}) \\ &+ \widehat{J_{\omega_f}}\widehat{L}\left(\delta_{nn_f}\begin{Bmatrix} j_f & L & j_{n_i} \\ j_p & J_{\omega_f} & j_n\end{Bmatrix} u_pv_nX^{\omega_f}_{pn_i} - \delta_{nn_i}\frac{\delta_{j_fj_p}}{\widehat{j_f}^2}v_pu_nY^{\omega_f}_{pn_f}\right)\Bigg]\end{aligned} \tag{B.3}$$

and

$$\begin{aligned}&(n_f\omega_f; j_f\|[c_p^\dagger \tilde{c}_n]_L\|p_i\omega_i; j_i) \\ &\quad= (-1)^{j_{p_i}+j_i+J_{\omega_i}}v_pv_n\widehat{j_i}\widehat{j_f}\widehat{L}\Bigg(\delta_{pp_i}\delta_{nn_f}\delta_{\omega_i\omega_f}\begin{Bmatrix} j_f & L & j_i \\ j_p & J_{\omega_i} & j_n\end{Bmatrix} - \widehat{J_{\omega_i}}\widehat{J_{\omega_f}} \\ &\times\Bigg[\delta_{pp_i}\begin{Bmatrix} j_f & L & j_i \\ j_p & J_{\omega_i} & j_n\end{Bmatrix}\sum_{p'}\left(\begin{Bmatrix} j_f & J_{\omega_f} & j_{n_f} \\ j_{p'} & J_{\omega_i} & j_n\end{Bmatrix}X^{\omega_f}_{p'n}X^{\omega_i}_{p'n_f} - \frac{\delta_{j_fj_{p'}}}{\widehat{j_f}^2}Y^{\omega_f}_{p'n_f}Y^{\omega_i}_{p'n}\right) \\ &+ \delta_{nn_f}\begin{Bmatrix} j_f & L & j_i \\ j_p & J_{\omega_f} & j_n\end{Bmatrix}\sum_{n'}\left(\begin{Bmatrix} j_{p_i} & J_{\omega_i} & j_i \\ j_p & J_{\omega_f} & j_{n'}\end{Bmatrix}X^{\omega_f}_{p_in'}X^{\omega_i}_{pn'} - \frac{\delta_{j_ij_{n'}}}{\widehat{j_i}^2}Y^{\omega_f}_{pn'}Y^{\omega_i}_{p_in'}\right) \\ &\qquad+ \begin{Bmatrix} j_{n_f} & J_{\omega_f} & j_f \\ j_p & j_n & L \\ J_{\omega_i} & j_{p_i} & j_i\end{Bmatrix}X^{\omega_f}_{p_in}X^{\omega_i}_{pn_f} + \frac{\delta_{j_ij_n}\delta_{j_fj_p}}{\widehat{j_i}^2\,\widehat{j_f}^2}Y^{\omega_f}_{pn_f}Y^{\omega_i}_{p_in}\Bigg]\Bigg).\end{aligned} \tag{B.4}$$

The pnMPQM β^- CCTDs from a proton-odd to a neutron-odd nucleus are

$$(n_f\|[c_p^\dagger\tilde{c}_n]_L\|p_i) = \delta_{pp_i}\delta_{nn_f}(-1)^{j_p+j_n+L}\widehat{L}v_pv_n, \tag{B.5}$$

$$(n_f\|[c_p^\dagger\tilde{c}_n]_L\|n_i\omega_i;j_i) = (-1)^{j_{n_f}+L+j_i+1}\widehat{j_i}\Bigg[\delta_{n_in_f}\delta_{J_{\omega_i}L}(v_pu_nX_{pn}^{\omega_i}+u_pv_nY_{pn}^{\omega_i}) + \widehat{J_{\omega_i}}\widehat{L}\left(\delta_{nn_i}\begin{Bmatrix} j_{n_f} & L & j_i \\ j_n & J_{\omega_i} & j_p\end{Bmatrix}v_pu_nX_{pn_f}^{\omega_i} - \delta_{nn_f}\frac{\delta_{j_ij_p}}{\widehat{j_i}^2}u_pv_nY_{pn_i}^{\omega_i}\right)\Bigg], \tag{B.6}$$

$$(p_f\omega_f;j_f\|[c_p^\dagger\tilde{c}_n]_L\|p_i) = (-1)^{j_{p_i}+j_{p_f}+J_{\omega_f}+L+1}\widehat{j_f}\Bigg[\delta_{p_ip_f}\delta_{J_{\omega_f}L}(u_pv_nX_{pn}^{\omega_f}+v_pu_nY_{pn}^{\omega_f}) + \widehat{J_{\omega_f}}\widehat{L}\left(\delta_{pp_f}\begin{Bmatrix} j_f & L & j_{p_i} \\ j_n & J_{\omega_f} & j_p\end{Bmatrix}u_pv_nX_{p_in}^{\omega_f} - \delta_{pp_i}\frac{\delta_{j_fj_n}}{\widehat{j_f}^2}v_pu_nY_{p_fn}^{\omega_f}\right)\Bigg] \tag{B.7}$$

and

$$\begin{aligned}(p_f\omega_f;j_f\|[c_p^\dagger\tilde{c}_n]_L\|n_i\omega_i;j_i) &= (-1)^{j_i+j_{p_f}+J_{\omega_f}+L+1}u_pu_n\widehat{j_i}\widehat{j_f}\widehat{L}\Bigg(\delta_{\omega_i\omega_f}\delta_{pp_f}\delta_{nn_i}\begin{Bmatrix} j_f & L & j_i \\ j_n & J_{\omega_i} & j_p\end{Bmatrix} - \widehat{J_{\omega_i}}\widehat{J_{\omega_f}} \\ &\times\Bigg[\delta_{pp_f}\begin{Bmatrix} j_f & L & j_i \\ j_n & J_{\omega_f} & j_p\end{Bmatrix}\sum_{p'}\left(\begin{Bmatrix} j_{n_i} & J_{\omega_i} & j_i \\ j_n & J_{\omega_f} & j_{p'}\end{Bmatrix}X_{p'n_i}^{\omega_f}X_{p'n}^{\omega_i} - \frac{\delta_{j_ij_{p'}}}{\widehat{j_i}^2}Y_{p'n}^{\omega_f}Y_{p'n_i}^{\omega_i}\right) \\ &+\delta_{nn_i}\begin{Bmatrix} j_f & L & j_i \\ j_n & J_{\omega_i} & j_p\end{Bmatrix}\sum_{n'}\left(\begin{Bmatrix} j_f & J_{\omega_f} & j_{p_f} \\ j_{n'} & J_{\omega_i} & j_p\end{Bmatrix}X_{pn'}^{\omega_f}X_{p_fn'}^{\omega_i} - \frac{\delta_{j_fj_{n'}}}{\widehat{j_f}^2}Y_{p_fn'}^{\omega_f}Y_{pn'}^{\omega_i}\right) \\ &+\begin{Bmatrix} J_{\omega_f} & j_{p_f} & j_f \\ j_p & j_n & L \\ j_{n_i} & J_{\omega_i} & j_i\end{Bmatrix}X_{pn_i}^{\omega_f}X_{p_fn}^{\omega_i} + \frac{\delta_{j_ij_p}\delta_{j_fj_n}}{\widehat{j_i}^2\widehat{j_f}^2}Y_{p_fn}^{\omega_f}Y_{pn_i}^{\omega_i}\Bigg]\Bigg).\end{aligned} \tag{B.8}$$

The CCTDs for β^+ and electron capture decays from a neutron-odd to a proton-odd nucleus read

$$(p_f\|[c_n^\dagger\tilde{c}_p]_L\|n_i) = \delta_{pp_f}\delta_{nn_i}(-1)^{j_p+j_n+L}\widehat{L}v_pv_n, \tag{B.9}$$

$$(p_f\|[c_n^\dagger\tilde{c}_p]_L\|p_i\omega_i;j_i) = (-1)^{j_p+j_n+j_{p_i}+J_{\omega_i}+j_i+L}\widehat{j_i}\Bigg[\delta_{p_ip_f}\delta_{J_{\omega_i}L}(u_pv_nX_{pn}^{\omega_i}+v_pu_nY_{pn}^{\omega_i}) + \widehat{J_{\omega_i}}\widehat{L}\left(\delta_{pp_i}\begin{Bmatrix} j_{p_f} & L & j_i \\ j_p & J_{\omega_i} & j_n\end{Bmatrix}u_pv_nX_{p_fn}^{\omega_i} - \delta_{pp_f}\frac{\delta_{j_ij_n}}{\widehat{j_i}^2}v_pu_nY_{p_in}^{\omega_i}\right)\Bigg], \tag{B.10}$$

$$(n_f\omega_f; j_f\|c_n^\dagger\tilde{c}_p]_L\|n_i) = (-1)^{j_p+j_n+L+1}\widehat{j_f}\Bigg[\delta_{n_in_f}\delta_{J_{\omega_f}L}(v_pu_nX_{pn}^{\omega_f} + u_pv_nY_{pn}^{\omega_f}) + \widehat{J_{\omega_f}}\widehat{L}\left(\delta_{nn_f}\begin{Bmatrix} j_f & L & j_{n_i} \\ j_p & J_{\omega_f} & j_n \end{Bmatrix} v_pu_nX_{pn_i}^{\omega_f} - \delta_{nn_i}\frac{\delta_{j_fj_p}}{\widehat{j_f}^2}u_pv_nY_{pn_f}^{\omega_f}\right)\Bigg] \quad \text{(B.11)}$$

and

$$\begin{aligned}(n_f\omega_f; j_f\|c_n^\dagger\tilde{c}_p]_L\|p_i\omega_i; j_i) &= (-1)^{j_p+j_n+L+j_{p_i}+j_i+J_{\omega_i}}u_pu_n\widehat{j_i}\widehat{j_f}\widehat{L}\Bigg(\delta_{pp_i}\delta_{nn_f}\delta_{\omega_i\omega_f}\begin{Bmatrix} j_f & L & j_i \\ j_p & J_{\omega_i} & j_n \end{Bmatrix} - \widehat{J_{\omega_i}}\widehat{J_{\omega_f}} \\ &\times\Bigg[\delta_{pp_i}\begin{Bmatrix} j_f & L & j_i \\ j_p & J_{\omega_i} & j_n \end{Bmatrix}\sum_{p'}\left(\begin{Bmatrix} j_f & J_{\omega_i} & j_n \\ j_{p'} & J_{\omega_f} & j_{n_f} \end{Bmatrix}X_{p'n}^{\omega_f}X_{p'n_f}^{\omega_i} - \frac{\delta_{j_fj_{p'}}}{\widehat{j_f}^2}Y_{p'n_f}^{\omega_f}Y_{p'n}^{\omega_i}\right) \\ &+ \delta_{nn_f}\begin{Bmatrix} j_f & L & j_i \\ j_p & J_{\omega_f} & j_n \end{Bmatrix}\sum_{n'}\left(\begin{Bmatrix} j_p & J_{\omega_f} & j_i \\ j_{p_i} & J_{\omega_i} & j_{n'} \end{Bmatrix}X_{p_in'}^{\omega_f}X_{pn'}^{\omega_i} - \frac{\delta_{j_ij_{n'}}}{\widehat{j_i}^2}Y_{pn'}^{\omega_f}Y_{p_in'}^{\omega_i}\right) \\ &+ \begin{Bmatrix} J_{\omega_f} & j_{n_f} & j_f \\ j_n & j_p & L \\ j_{p_i} & J_{\omega_i} & j_i \end{Bmatrix}X_{p_in}^{\omega_f}X_{pn_f}^{\omega_i} + \frac{\delta_{j_ij_n}\delta_{j_fj_p}}{\widehat{j_i}^2\,\widehat{j_f}^2}Y_{pn_f}^{\omega_f}Y_{p_in}^{\omega_i}\Bigg]\Bigg). \quad \text{(B.12)}\end{aligned}$$

Finally, the CCTDs for the β^+/EC decays for the transition from a proton-odd to a neutron-odd nucleus are

$$(n_f\|[c_n^\dagger\tilde{c}_p]_L\|p_i) = \delta_{pp_i}\delta_{nn_f}\widehat{L}u_pu_n, \quad \text{(B.13)}$$

$$(n_f\|[c_n^\dagger\tilde{c}_p]_L\|n_i\omega_i; j_i) = (-1)^{j_p+j_n+j_{n_f}+j_i}\widehat{j_i}\Bigg[\delta_{n_in_f}\delta_{J_{\omega_i}L}(u_pv_nX_{pn}^{\omega_i} + v_pu_nY_{pn}^{\omega_i}) + \widehat{J_{\omega_i}}\widehat{L}\left(\delta_{nn_i}\begin{Bmatrix} j_{n_f} & L & j_i \\ j_n & J_{\omega_i} & j_p \end{Bmatrix}u_pv_nX_{pn_f}^{\omega_i} - \delta_{nn_f}\frac{\delta_{j_ij_p}}{\widehat{j_i}^2}v_pu_nY_{pn_i}^{\omega_i}\right)\Bigg], \quad \text{(B.14)}$$

$$(p_f\omega_f; j_f\|[c_n^\dagger\tilde{c}_p]_L\|p_i) = (-1)^{j_p+j_n+j_{p_i}+j_{p_f}+J_{\omega_f}}\widehat{j_f}\Bigg[\delta_{p_ip_f}\delta_{J_{\omega_f}L}(v_pu_nX_{pn}^{\omega_f} + u_pv_nY_{pn}^{\omega_f}) + \widehat{J_{\omega_f}}\widehat{L}\left(\delta_{pp_f}\begin{Bmatrix} j_f & L & j_{p_i} \\ j_n & J_{\omega_f} & j_p \end{Bmatrix}v_pu_nX_{p_in}^{\omega_f} - \delta_{pp_i}\frac{\delta_{j_fj_n}}{\widehat{j_f}^2}u_pv_nY_{p_fn}^{\omega_f}\right)\Bigg] \quad \text{(B.15)}$$

and

$$
\begin{aligned}
&(p_f\omega_f; j_f \| [c_n^\dagger \tilde{c}_p]_L \| n_i\omega_i; j_i) \\
&\quad = (-1)^{j_p+j_n+j_{p_f}+j_i+J_{\omega_f}+1} v_p v_n \widehat{j_i}\widehat{j_f}\widehat{L} \Bigg(\delta_{pp_f}\delta_{nn_i}\delta_{\omega_i\omega_f} \begin{Bmatrix} j_f & L & j_i \\ j_n & J_{\omega_i} & j_p \end{Bmatrix} - \widehat{J_{\omega_i}}\widehat{J_{\omega_f}} \\
&\quad \times \Bigg[\delta_{pp_f} \begin{Bmatrix} j_f & L & j_i \\ j_n & J_{\omega_f} & j_p \end{Bmatrix} \sum_{p'} \Bigg(\begin{Bmatrix} j_n & J_{\omega_f} & j_i \\ j_{n_i} & J_{\omega_i} & j_{p'} \end{Bmatrix} X^{\omega_f}_{p'n_i} X^{\omega_i}_{p'n} - \frac{\delta_{j_i j_{p'}}}{\widehat{j_i}^2} Y^{\omega_f}_{p'n} Y^{\omega_i}_{p'n_i} \Bigg) \\
&\quad + \delta_{nn_i} \begin{Bmatrix} j_f & L & j_i \\ j_n & J_{\omega_i} & j_p \end{Bmatrix} \sum_{n'} \Bigg(\begin{Bmatrix} j_f & J_{\omega_i} & j_p \\ j_{n'} & J_{\omega_f} & j_{p_f} \end{Bmatrix} X^{\omega_f}_{pn'} X^{\omega_i}_{p_f n'} - \frac{\delta_{j_f j_{n'}}}{\widehat{j_f}^2} Y^{\omega_f}_{p_f n'} Y^{\omega_i}_{pn'} \Bigg) \\
&\qquad\qquad + \begin{Bmatrix} J_{\omega_f} & j_{p_f} & j_f \\ j_p & j_n & L \\ j_{n_i} & J_{\omega_i} & j_i \end{Bmatrix} X^{\omega_f}_{pn_i} X^{\omega_i}_{p_f n} + \frac{\delta_{j_i j_p}\delta_{j_f j_n}}{\widehat{j_i}^2\,\widehat{j_f}^2} Y^{\omega_f}_{p_f n} Y^{\omega_i}_{pn_i} \Bigg] \Bigg). \quad \text{(B.16)}
\end{aligned}
$$